Received 13 February 2024; accepted 27 March 2024. Date of publication 4 April 2024; date of current version 22 April 2024.

Digital Object Identifier 10.1109/OJCOMS.2024.3384988

Achieving Capacity Gains in Practical Full-Duplex Massive MIMO Systems: A Multi-Objective Optimization Approach Using Hybrid Beamforming

MOBEEN MAHMOOD (Graduate Student Member, IEEE), ASIL KOC (Graduate Student Member, IEEE), ROBERT MORAWSKI, AND THO LE-NGOC (Life Fellow, IEEE)

Department of Electrical and Computer Engineering, McGill University, Montreal, QC H3A 0G4, Canada

CORRESPONDING AUTHOR: M. MAHMOOD (e-mail: mobeen.mahmood@mail.mcgill.ca)

This work was supported in part by Huawei Technologies Canada, and in part by the Natural Sciences and Engineering Research Council of Canada.

An earlier version of this paper has been presented in part at the 2023 IEEE Global Communications Conference [1] [DOI: 10.1109/GLOBECOM54140.2023].

ABSTRACT This paper presents a novel approach to full-duplex (FD) massive multiple-input multiple-output (mMIMO) systems using hybrid beamforming (HBF) architecture, enabling simultaneous uplink (UL) and downlink (DL) transmission within the same frequency band. The proposed solution aims to mitigate strong self-interference (SI) and maximize the total achievable rate based on over-the-air (OTA) measurements of the SI channel. Our objective is to leverage the spatial degrees of freedom (DoF) in mMIMO systems to enhance FD capacity without the need for expensive analog SI-cancellation circuitry. To address this challenging issue, we employ a sub-array configuration for transmit and receive antennas at the base station (BS) and design the RF stages using non-orthogonal beamforming (NOBF) in both UL and DL user directions. Additionally, sub-array selection (SAS) is utilized to identify the optimal Tx-Rx antenna pair. To solve the non-convex multi-objective optimization problem (MOOP), we propose a swarm intelligence-based algorithmic solution to determine the optimal perturbations in user directions jointly with Tx-Rx sub-array indices while satisfying directivity degradation constraints. The illustrative results show that the proposed NOBF scheme with SAS can achieve an SI suppression of −78 dB. Furthermore, in FD mMIMO systems, this approach can effectively double the capacity compared to half-duplex (HD) transmissions.

INDEX TERMS Full-duplex (FD), hybrid beamforming (HBF), massive MIMO, multi-objective optimization problem (MOOP), self-interference suppression.

I. INTRODUCTION

MASSIVE multiple-input multiple-output (mMIMO), which is a pivotal enabler of fifth-generation (5G) networks, utilizes large array structures at the base station (BS) to serve multiple users via spatial multiplexing. Full-duplex (FD) communications offer significant performance gains compared to half-duplex (HD) communications by offering simultaneous uplink (UL) and downlink (DL) transmission of signals at the same frequency and time resources. Thus, FD communications have the potential to meet the ever-increasing demand of data traffic for future wireless communications systems [2]. However, to fully exploit the advantages of FD communications, the key challenging issue is to suppress the strong self-interference (SI) due to the coupling of the transmit signal with the receiver chains [3]. The use of large array structures both at the transmitter (Tx) and receiver (Rx) in FD communications can provide additional spatial degrees of freedom (DoF), which can help to suppress strong SI and can double the capacity. Thus, FD and mMIMO can fulfill the throughput and latency demands of future wireless communications systems with limited spectrum resources [4].

Many research studies have focused on SI suppression to fully utilize the FD technology [5], [6], [7]. The Tx and Rx antenna sub-systems can be designed in such a way to isolate the transmit and receive RF chains as much as possible [8], [9], [10]. The practical demonstrations show SI suppression between -60 and −70 dB based on antenna

isolation [11]. On the other hand, active SI cancellation refers to mitigating SI by subtracting a processed copy of the transmitted signal from the received signal. Then, based on the signal domain, where the SI signal is subtracted, active cancellation is divided into digital and analog SI cancellations. Analog SI cancellation requires the use of specially designed circuitry to reconstruct the SI counterpart and subtract it from the received signal at the analog front-end of the local Rx [12], [13], [14]. Digital SI cancellation techniques are considered to be the simplest forms of active cancellation techniques. However, the amount of SI cancellation achieved through digital techniques is quite limited due to hardware imperfections, particularly transceiver phase noise and non-linearities that restrict the performance of traditional digital cancellation techniques [15]. Therefore, antenna isolation, analog SI suppression/cancellation, digital SI cancellation, and their combinations have been used to suppress the strong SI signal below the Rx noise floor in FD communications [16], [17], [18].

In 5G and beyond 5G (B5G) systems, there is a growing trend towards utilizing an increased number of antennas at BS. For instance, the third-generation partnership project (3GPP) has been considering configurations with 64-256 antennas [19]. However, the increased number of antennas introduces additional challenges for analog SI cancellation in FD mMIMO systems. This results in high analog complexity, which is not affordable. An alternative approach relies exclusively on transmit beamforming to suppress SI, thereby completely obviating the need for analog cancelers [20]. In mMIMO HD systems, fully-digital beamforming (FDBF) and hybrid beamforming (HBF) are two common approaches for reducing interference. Recent studies, for instance, SoftNull [20], have exploited the availability of multiple antennas in FD mMIMO systems to achieve SIC via FDBF, known as spatial suppression. However, FDBF becomes infeasible for mMIMO systems with very large array structures due to prohibitively high cost, complexity and energy consumption. On the other hand, HBF, which combines both radio frequency (RF) and baseband (BB) stages, can approach the performance of FDBF by reducing the number of energy-intensive RF chains, thus minimizing power consumption.

A. STATE-OF-THE-ART AND MOTIVATION

Several HBF approaches have been investigated for both HD and FD transmissions in related research [21], [22], [23], [24], [25], [26], [27], [28], [29], [30], [31], [32], [33], [34], [35], [36], [37], [38]. In HD transmission studies [21], [22], [23], [24], [25], [26], [27], [28], [29], hybrid precoding in DL and hybrid combining in UL have been examined. In particular, the authors in [21] propose a joint design of RF and BB stages using full channel state information (CSI) to maximize the system's total sum-rate. Reference [22] employs singular value decomposition (SVD)-based HBF for millimeter-wave (mmWave) mMIMO systems, whereas an alternating optimization approach is proposed in [23] for fully-connected (FC) and sub-array-connected (SC) HBF structures. An angular-based HBF technique is proposed in [24], where the RF-stage is constructed utilizing users' angular information only. In [25], the authors propose a sub-connected HBF structure where each Tx and Rx consists of several sub-arrays, and the total achievable rate is maximized using the successive interference cancellation technique. An eigen beamforming-based HBF techniques are developed in [26], [27], [28], utilizing the channel covariance matrix. These techniques investigate different two-dimensional (2D) array structures with full and low-resolution hardware components. The authors then extend their work in [29] for different three-dimensional (3D) array configurations in mMIMO systems, where HBF is designed using SVD of the channel matrix.

Regarding the FD communications in mMIMO systems, an 8×8 Tx/8×8 Rx antenna array prototype is designed in [30] for sub-6GHz frequency band, which can achieve an average SI suppression of -65.6 dB. A hybrid precoding/combining (HPC) technique for mmWave FD mMIMO systems is proposed in [31], which uses the angle-of-departure (AoD) and angle-of-arrival (AoA) information to suppress SI while also reducing the number of RF chains. The authors show that the power of far-field SI channel is suppressed by -81.5 dB, whereas the near-field SI power is reduced by -44.5 dB in point-to-point FD mMIMO systems. In [32], separate and joint FD beamforming algorithms based on sequential convex programming are presented to maximize the sum-rate for both single-user (SU)- or multi-user (MU)-MIMO FD systems. In [33], a FD mmWave relaying system is considered to suppress SI while maximizing spectral efficiency using an orthogonal matching pursuit-based SI-cancellation algorithm. Similarly, a HPC design for FD amplify-and-forward (AF) mmWave relay system is considered in [34], introducing a zero-space SI cancellation method based on correlated mmWave channel estimation errors. A FD mmWave HBF scheme is introduced in [35] for a MU-mMIMO systems, where the non-orthogonal beams are generated to serve multiple users while suppressing the near-field component of the SI channel and maximizing the sum-rate capacity. The authors show that the proposed HBF scheme can reduce SI by 78.1 dB in FD mMIMO systems. In [36], the authors proposed an iterative FD HBF scheme to mitigate SI by jointly designing the transmit and receive RF beamformer weights, the precoder, and combiner matrices and achieving SI suppression by up to 30 dB. The authors in [37] designed the analog and digital beamformers of a FD mMIMO systems based on the practical constraints of RF chains, channel knowledge, beam alignment, and a limited receive dynamic range. A two-timescale HBF scheme for FD mmWave multiple-relay transmission is investigated in [38], where the analog and digital beams are updated based on channel samples and real-time low-dimensional effective channel state information (CSI) matrices, respectively.

The existing research studies, for instance [31], [32], [33], [34], [35], [36], [37], [38], consider HBF in FD mMIMO systems to mitigate the strong SI from Tx to Rx. However, the SI suppression evaluation in these studies relies exclusively on the theoretical SI channel models. In other words, the studies in [31], [32], [33], [34], [35], [36], [37], [38] do not consider the experimental evaluations to validate the theoretical doubling of capacity/throughput. Instead, the studies assume both residual near-field SI channel via line-of-sight (LoS) paths and the far-field SI channel via the reflected non-line-of-sight (NLoS) paths in a simulated manner. In practical implementations, real-world platforms inevitably experience a signal-to-interference-plus-noise ratio (SINR) loss due to the impact of strong SI. Therefore, it is important to develop a robust understanding of beamforming-based SI suppression capabilities by utilizing the experimentally measured SI channels. Therefore, investigating the effectiveness of beamforming-based SI suppression in the real-time implementation of FD mMIMO systems becomes essential to bridge this gap between theory and practical performance.

Additionally, most existing FD studies primarily consider FC-HBF architectures. In the FC-HBF scheme, each RF chain is connected to all antenna elements, which allows the RF chain to exploit the full beamforming capability of the antenna array. However, this leads to increased cost and complexity. On the other hand, SC-HBF architectures require the connection of each RF chain to a subset of antennas, significantly reducing the connectivity and implementation cost/complexity. Thus, SC-HBF utilizes fewer RF phase shifters (PSs) circuits compared to FC-HBF, and its use can reduce power consumption at the expense of some performance degradation. However, SC-HBF can provide a better spectral-energy efficiency tradeoff [39], [40]. Thus, it is more suitable to deploy SC-HBF structure for future key enabling technologies, for instance, mmWave and sub-Terahertz (THz) communications [41], [42], [43]. It is worth noting that the SC-HBF architecture is mainly considered in HD transmission studies, while most research in FD communications has focused on the use of FC-HBF [31], [32], [33], [34], [35], [36], [37], [38]. Therefore, it is important to explore SC-HBF architecture's potential in FD mMIMO systems in order to reveal its advantages and enable its deployment in emerging technologies.

B. CONTRIBUTIONS

This research aims to perform a data-driven analysis of the FD architecture proposed in [35]. Based on the extensive experimental data, our main contribution lies in enhancing the capacity of a practical FD system by mitigating SI through the beamforming capability of the SC-HBF architecture. In [1], a novel sub-array selection (SAS) scheme is proposed, which minimizes the SI for a single-objective optimization problem (SOOP) in FD mMIMO systems. This research work addresses a multi-objective optimization problem (MOOP) of reducing SI while maximizing the total achievable rate in real-time FD mMIMO systems. Compared to the existing studies based on theoretical SI channel models, we leverage over-the-air (OTA) measured SI channel data. To the best of our knowledge, this is the first work to consider SI suppression and achievable rate maximization exclusively through the design of Tx and Rx RF beamforming stages jointly with SAS, and employs a measured SI channel in an anechoic chamber. Our objective here is to show that only using the spatial DoF provided due to the use of large array structures is capable of bringing the SI level down to the noise floor, thus avoiding the use of costly/complex analog cancellation circuits. Also, unlike prior literature for FD studies, which consider FC-HBF, this study considers a SC-HBF architecture, which can reduce power consumption and can contribute towards understanding beamforming-based SI suppression capability for future mmWave and sub-THz systems using SC architectures. The main contributions of this work are summarized as follows:

1) We formulate a multi-objective optimization framework that focuses on maximizing the total achievable-rate and SI minimization in FD mMIMO systems. To solve this challenging non-convex MOOP, we propose swarm intelligence-based SI suppression scheme that optimizes the beam perturbations in the UL and DL UE directions and find the best Tx and Rx sub-arrays while satisfying the directivity degradation constraints.
2) We propose two different SI suppression schemes for the design of UL/DL RF beamformers, namely orthogonal beamforming (OBF) and non-orthogonal beamforming (NOBF) incorporating SAS for MOOP.[1] The OBF scheme optimizes the RF beamformers by maximizing the intended signal power and suppressing SI leakage power using orthogonal beams. In the joint NOBF with SAS scheme, we introduce perturbations to the orthogonal beams to enhance SI suppression. Compared to the NOBF scheme in [35], which uses phase-range constraints, the proposed NOBF scheme uses directivity-loss constraints, which offer greater flexibility in perturbing the orthogonal beams while maintaining low directivity loss. Additionally, we jointly select the best Tx and Rx sub-arrays, optimizing the UL and DL beam directions to further enhance SI suppression by leveraging the spatial DoF.
3) For the practical application purpose, we implement a testbed in an anechoic chamber to measure the SI channel in the sub-6GHz band. The experimental setup considers 64 Tx and 64 Rx antenna elements as per 3GPP [19] and the measurements are done without external surrounding reflections (i.e., SI channel is mainly due to "internal" coupling between Tx and Rx antenna arrays) for a frequency band between 3 GHz and 4 GHz. We formulate RF beamforming

[1]It must be noted that the OBF and NOBF RF beamformers design in [1] reduces SI only, whereas, in this work, the OBF and NOBF RF beamformers formulation is based on a multi-objective design criteria, i.e., reducing SI and maximizing the total rate.

stages using the proposed perturbation-based NOBF schemes using the measured SI channel for 20 MHz bandwidth (BW). Moreover, we employ a SC-HBF architecture for both Tx and Rx arrays, and investigate SI suppression for the measured SI channel. The illustrative results show the significant SI suppression achieved using the proposed joint NOBF with SAS scheme compared to the OBF scheme. We also demonstrate that using only 4 (1×4) or 8 (1×8) antenna elements, SI value can be brought down to −78 dB, which shows the spatial suppression abilities of FD mMIMO systems.

4) We provide a realistic capacity gain in FD communications compared to HD transmissions in mMIMO systems. Specifically, we consider the extreme case when both UL and DL users are at same angular locations. Our results show that FD performance degrades significantly when using OBF scheme due to inter-user interference (IUI). However, using the proposed joint NOBF with SAS scheme can achieve approximately 1.85 times more capacity than HD communications in real-time implementations.

C. ORGANIZATION

The rest of this paper is organized as follows. Section II presents the system and channel models for the FD mMIMO systems. Section III discusses the Tx and Rx sub-array mapping and the problem formulation. Section IV presents the proposed HBF schemes using OBF and NOBF RF beamformers jointly with SAS, followed by the illustrative results in Section V. Finally, Section VI concludes the paper.

Notation: The following notations are used throughout this paper. Boldface lower-case and upper-case letters denote column vectors and matrices, respectively. $(\cdot)^T$, $(\cdot)^H$ and $\|.\|$ represent the transpose, complex-transpose, and the 2-norm of a vector or matrix, respectively. $\mathbf{I}_k$, $\mathbb{E}[.]$ and tr(.) denote $k \times k$ identity matrix, the expectation operator and the trace operator, respectively. We use $x_k \sim \mathcal{CN}(0, \sigma)$ when x_k is a complex Gaussian random variable with zero-mean and variance σ.

II. SYSTEM AND CHANNEL MODEL

In this section, we present the system and channel models for the FD mMIMO systems using SC-HBF architecture.

A. SYSTEM MODEL

We consider a single-cell FD mMIMO systems for joint DL and UL transmission as shown in Fig. 2. Here, the BS is equipped with transmit/receive uniform rectangular arrays (URAs), and operates in FD mode to simultaneously serve K_D DL and K_U UL single-antenna users over the same frequency band, while the users operate in HD mode due to the hardware/software constraints (e.g., low power consumption, limited signal processing and active/passive SI suppression capability). Specifically, the transmit (receive)

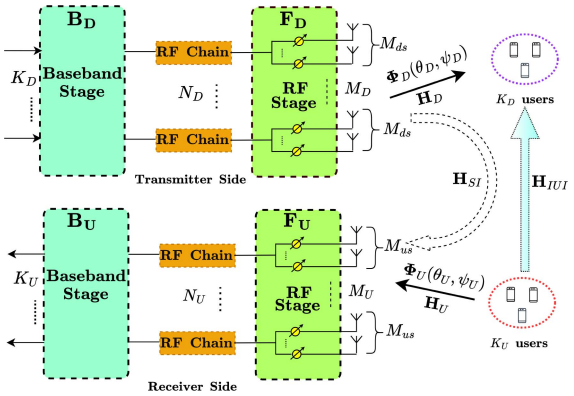

FIGURE 1. FD mMIMO system using SC-HBF architecture.

URA has $M_D = M_D^{(x)} \times M_D^{(y)} (M_U = M_U^{(x)} \times M_U^{(y)})$ antennas, where $M_D^{(x)}(M_U^{(x)})$ and $M_D^{(y)}(M_U^{(y)})$ denote the number of transmit (receive) antennas along x-axis and y-axis, respectively.

For the proposed FD mMIMO systems, we consider the DL signal is processed through DL BB stage $\mathbf{B}_D = [\mathbf{b}_{D,1}, \mathbf{b}_{D,2}, \ldots, \mathbf{b}_{D,K_D}] \in \mathbb{C}^{N_D \times K_D}$ and DL RF beamformer $\mathbf{F}_D \in \mathbb{C}^{M_D \times N_D}$, where N_D is the number of RF chains such that $K_D \leq N_D \ll M_D$ and $\mathbf{b}_{D,k} \in N_D$ is the BB stage vector for k^{th} DL UE. Similarly, the received UL signal at BS is processed through UL RF beamformer $\mathbf{F}_U \in \mathbb{C}^{N_U \times M_U}$ and UL BB combiner $\mathbf{B}_U = [\mathbf{b}_{U,1}, \mathbf{b}_{U,2}, \ldots, \mathbf{b}_{U,K_U}]^T \in \mathbb{C}^{K_U \times N_U}$ by utilizing $K_U \leq N_U \ll M_U$ RF chains. To further reduce the complexity and cost, we consider a SC-HBF architecture as shown in Fig. 2, where the Tx (Rx) URA is divided into $L_D(L_U)$ different sub-arrays in the form of uniform linear array (ULA). Hence, compared to $M_D \times N_D$ PSs for Tx ($M_U \times N_U$ PSs for Rx), only $M_{ds} \times N_D (M_{us} \times N_U)$ PSs are required as RF chain s is connected to a specific sub-array, comprising a distinct set of antenna elements. Here, $M_{ds}(M_{us})$ represents the number of Tx (Rx) antenna elements for RF chain s, where $\sum_{s=1}^{L_D} M_{ds} = M_D$ and $\sum_{s=1}^{L_U} M_{us} = M_U$. The l_D^{th} Tx sub-array, for instance, consists of M_{ds} antenna elements numbered from 1 to M_{ds}, ensuring a sequential distribution of elements within each sub-array. Similarly, the l_U^{th} Rx sub-array comprises antenna elements numbered from 1 to M_{us}. This approach ensures an orderly arrangement of antenna elements within each sub-array. We assume that $M_{ds}(M_{us})$ is an integer value such that each Tx (Rx) sub-array has the same number of antennas. It must be noted that each sub-array is independent of each other. Thus, we can write the DL and UL RF beamformers as follows:

$$\mathbf{F}_D = \begin{bmatrix} \mathbf{f}_D^{(1)} & \mathbf{0} & \ldots & \mathbf{0} \\ \mathbf{0} & \mathbf{f}_D^{(2)} & \ldots & \mathbf{0} \\ \vdots & \vdots & \ddots & \vdots \\ \mathbf{0} & \mathbf{0} & \ldots & \mathbf{f}_D^{(L_D)} \end{bmatrix} \in \mathbb{C}^{M_D \times N_D}, \quad (1)$$

$$\mathbf{F}_U = \begin{bmatrix} \mathbf{f}_U^{(1)} & \mathbf{0} & \dots & \mathbf{0} \\ \mathbf{0} & \mathbf{f}_U^{(2)} & \dots & \mathbf{0} \\ \vdots & \vdots & \ddots & \vdots \\ \mathbf{0} & \mathbf{0} & \dots & \mathbf{f}_U^{(L_U)} \end{bmatrix}^H \in \mathbb{C}^{N_U \times M_U}, \quad (2)$$

where $\mathbf{f}_D^{(l_D)} \in \mathbb{C}^{M_{ds}}$ is the DL RF beamformer associated with l_D^{th} Tx sub-array. Similarly, $\mathbf{f}_U^{(l_U)} \in \mathbb{C}^{M_{us}}$ is the UL RF beamformer associated with l_U^{th} Rx sub-array. Here, the UL and DL RF beamforming stages (i.e., $\mathbf{F}_U$ and $\mathbf{F}_D$) are built using low-cost PSs, which brings the constant-modulus (CM) constraint due to the use of PSs. Then, the DL channel matrix is denoted as $\mathbf{H}_D = [\mathbf{h}_{D,1}, \mathbf{h}_{D,2}, \dots, \mathbf{h}_{D,K_D}]^T \in \mathbb{C}^{K_D \times M_D}$ with $\mathbf{h}_{D,d} \in \mathbb{C}^{M_D}$ as the d^{th} DL UE channel vector. Similarly, $\mathbf{H}_U = [\mathbf{h}_{U,1}, \mathbf{h}_{U,2}, \dots, \mathbf{h}_{U,K_U}] \in \mathbb{C}^{M_U \times K_U}$ is the UL channel matrix with $\mathbf{h}_{U,u} \in \mathbb{C}^{M_U}$ as the u^{th} UL UE channel vector. Due to the FD transmission, the SI channel matrix $\mathbf{H}_{\text{SI}} \in \mathbb{C}^{M_U \times M_D}$ is present between Tx and Rx antennas at the BS. For the DL transmission, the transmitted signal vector at the BS is defined as $\mathbf{s}_D = \mathbf{F}_D \mathbf{B}_D \mathbf{d}_D \in \mathbb{C}^{M_D}$, where $\mathbf{d}_D = [d_{D,1}, \dots, d_{D,K_D}]^T \in \mathbb{C}^{K_D}$ is the DL data signal vector such that $\mathbb{E}\{\mathbf{d}_D \mathbf{d}_D^H\} = \mathbf{I}_{K_D}$. The transmitted signal vector satisfies the maximum DL transmit power constraint, which is $\mathbb{E}\{||\mathbf{s}_D||^2\} = \text{tr}(\mathbf{F}_D \mathbf{B}_D \mathbf{B}_D^H \mathbf{F}_D^H) \leq P_D$, where P_D is the total DL transmit power. The IUI channel $\mathbf{H}_{\text{IUI}} = [\mathbf{h}_{\text{IUI},1}, \dots, \mathbf{h}_{\text{IUI},K_D}]^T \in \mathbb{C}^{K_D \times K_U}$ exists between DL and UL UEs, where $\mathbf{h}_{\text{IUI},d}$ denotes the channel vector from all UL UEs to the d^{th} DL UE. For the practical FD implementation, we consider the scenario of a single UL UE and a single DL UE (i.e., $K_D = K_U = 1$) to understand how close the FD systems can achieve in terms of theoretical doubling of the sum-rate capacity by suppressing strong measured SI based on beamforming capability of mMIMO systems.[2] Then, the received signal at the DL UE is given as follows:

$$r_D = \underbrace{\mathbf{h}_D^T \mathbf{f}_D \mathbf{b}_D d_D}_{\text{Desired Signal}} + \underbrace{\mathbf{h}_{\text{IUI}}^T d_U}_{\text{IUI by UL UE}} + \underbrace{w_D}_{\text{Noise}}, \quad (3)$$

where d_U is the UL data signal, $\mathbf{f}_D \in \mathbb{C}^{M_{ds} \times N_D}$ is the DL RF beamformer, and $w_D \sim \mathcal{CN}(0, \sigma_w^2)$ is the additive circular symmetric Gaussian noise. The received signal includes the desired DL signal, IUI generated by UL UE as well as the noise. Thus, the DL UE is exposed to IUI from UL UE due to the FD transmission. After some mathematical manipulations, we derive the instantaneous SINR at the DL UE as follows:

$$\text{SINR}_\text{D} = \frac{|\mathbf{h}_D^T \mathbf{f}_D \mathbf{b}_D|^2}{P_U ||\mathbf{h}_{\text{IUI}}||^2 + \sigma_\text{w}^2}. \quad (4)$$

[2]In this real-time FD implementation, we consider the scenario of single UL and a single DL UE to understand how effective SI suppression can be achieved solely based on beamforming capability with SAS based on a measured SI channel. The proposed perturbation-based NOBF scheme can be applied to the case of multiple UL and DL UEs in real-time systems, which is left as our future work.

Here, P_U is defined as the transmit power of UL UE. Similar to the DL data signal, the UL received signal at BS can be written as follows:

$$\tilde{r}_U = \underbrace{\mathbf{b}_U^T \mathbf{f}_U \mathbf{h}_U d_U}_{\text{Desired Signal}} + \underbrace{\mathbf{b}_U^T \mathbf{f}_U \mathbf{H}_{\text{SI}} \mathbf{f}_D \mathbf{b}_D \mathbf{d}_D}_{\text{SI}} + \underbrace{\tilde{\mathbf{w}_U}}_{\text{Modified Noise}}, \quad (5)$$

where $\tilde{\mathbf{w}_U} = \mathbf{b}_U \mathbf{f}_U \mathbf{w}_U$, $\mathbf{w}_U \sim \mathcal{CN}(0, \sigma_w^2 \mathbf{I}_{M_{us}})$ is the complex circularly symmetric Gaussian noise vector and $\mathbf{f}_U \in \mathbb{C}^{N_U \times M_{us}}$ is the UL RF beamformer. If $\boldsymbol{\mathcal{H}}_{\text{SI}} = \mathbf{f}_U \mathbf{H}_{\text{SI}} \mathbf{f}_D \in \mathbb{C}^{N_U \times N_D}$ is the effective SI channel seen from the BB-stage after applying DL and UL RF beamformers, then the instantaneous SINR for the UL UE can be given as:

$$\text{SINR}_\text{U} = \frac{\frac{P_U |\mathbf{b}_U^T \mathbf{f}_U \mathbf{h}_U|^2}{||\mathbf{b}_U^T \mathbf{f}_U||^2}}{\frac{||\mathbf{b}_U^T \boldsymbol{\mathcal{H}}_{\text{SI}} \mathbf{b}_D||^2}{||\mathbf{b}_U^T \mathbf{f}_U||^2} + \sigma_w^2}. \quad (6)$$

B. CHANNEL MODEL

In this subsection, we present the intended channel, measured SI channel in an anechoic chamber, and IUI channel.

1) INTENDED CHANNEL

Based on the geometry-based 3D channel model [44], the channel vector between the BS and UE is given by:

$$\mathbf{h}_i^T = \sum_{l=1}^{L} \tau_{i_l}^{-\eta} z_{i_l} \boldsymbol{\phi}_i(\theta_{i_l}, \psi_{i_l}) = \mathbf{z}_i^T \Phi_i \in \mathbb{C}^{M_i}, \quad (7)$$

where $\tau_{i_l}^{-n}$ and $z_{i_l} \sim \mathcal{CN}(0, \frac{1}{L})$ are the distance and complex path gain of the l^{th} path, η is the path loss exponent and $\boldsymbol{\phi}_i(..)$ is the array steering vector with $i = \{D, U\}$ is the DL phase response vector for $i = D$ or the UL phase response vector for $i = U$. Here, the angles $\theta_{i_l} \in [\theta_i - \delta_i^\theta, \theta_i + \delta_i^\theta]$ and $\psi_{i_l} \in [\psi_i - \delta_i^\psi, \psi_i + \delta_i^\psi]$ are the azimuth AoD (AAoD) and elevation AoD (EAoD) for l^{th} path in i^{th} channel, respectively. $\theta_i(\psi_i)$ is the mean AAoD(EAoD) with angular spread $\delta_i^\theta(\delta_i^\psi)$. Then, the i^{th} instantaneous channel vector for the user is represented via the fast time-varying path gain vector $\mathbf{z}_i = [\tau_{i_1}^{-\eta} z_{i_1}, \dots, \tau_{i_L}^{-\eta} z_{i_L}]^T \in \mathbb{C}^L$ and the slow time-varying phase response matrix as:

$$\Phi_i = \begin{bmatrix} \boldsymbol{\phi}_i^T(\theta_{i_1}, \psi_{i_1}) \\ \vdots \\ \boldsymbol{\phi}_i^T(\theta_{i_L}, \psi_{i_L}) \end{bmatrix} \in \mathbb{C}^{L \times M_i}, \quad (8)$$

where $M_i \in \{M_{ds}, M_{us}\}$ is the Tx/Rx antenna elements.

2) IUI CHANNEL

Based on the array phase response vectors $\boldsymbol{\phi}_D$ and $\boldsymbol{\phi}_U$ (as given in (8)), the IUI channel for single antenna u^{th} UL UE and d^{th} DL UE can be written as [35]:

$$\mathbf{H}_{\text{IUI}}(u, d) = \tau_{\text{IUI}_{u,d}}^{-\eta} z_{\text{IUI}_{u,d}}, \quad (9)$$

where $\tau_{\text{IUI}_{u,d}}$ and $z_{\text{IUI}_{u,d}} \sim \mathcal{CN}(0, 1)$ are the distance and path gain for the UL and DL UEs, respectively.

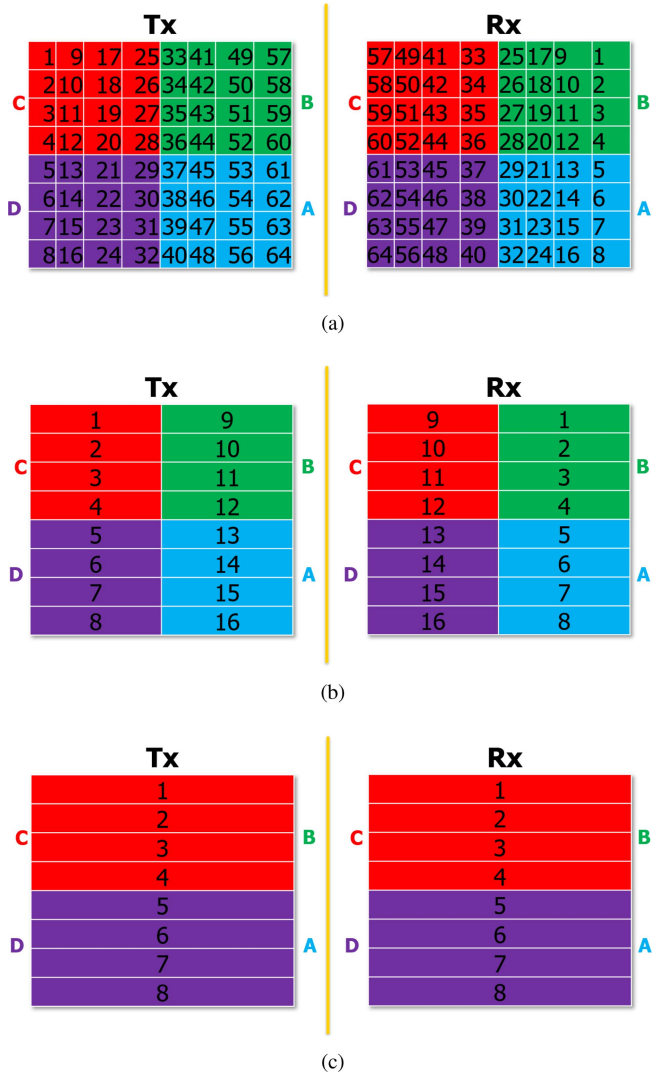

FIGURE 2. Antenna mapping. (a) 64 Tx and 64 Rx antennas index. (b) 1×4 Tx and Rx sub-array mapping. (c) 1×8 Tx and Rx sub-array mapping.

III. SUB-ARRAY MAPPING AND PROBLEM FORMULATION

In this section, we discuss the Tx and Rx sub-array mapping for the measured SI channel as well as the problem formulation using multiple optimization objectives.

A. SUB-ARRAY MAPPING

In Fig. 2(a), the antenna mapping is shown for both Tx and Rx of BS, which consists of $8\times8 = 64$ elements at BS and separated by an antenna isolation block. We present the sub-array mapping for our FD mMIMO setup in an anechoic chamber by using the following two different sub-array configurations for Tx and Rx: 1) 1×4 sub-array; and 2) 1×8 sub-array. Given 64 Tx and 64 Rx antenna elements, we can have 16 distinct Tx sub-arrays and similarly 16 Rx sub-arrays, each of 1×4 elements, which are arranged in the form of ULA. The mapping of the 1×4 sub-arrays for Tx and Rx ends can be represented mathematically as: Let $Tx(i,j)$ represent the (i,j)th element of the 8×8 Tx antenna array, where i denotes the row index and j denotes the column index. The mapping of the p^{th} 1×4 Tx sub-array, denoted as $Tx_{\text{sub},4}(p)$, can be expressed as follows:

$$Tx_{\text{sub},4}(p) = \left[Tx(i,j);\,(i,j) \in S_{p_4}\right], \tag{10}$$

where S_{p_4} represents the set of indices corresponding to the elements in the p^{th} 1×4 Tx sub-array. Similarly, let $Rx(i,j)$ represent the (i,j)th element of the 8×8 Rx antenna array. The mapping of the q^{th} 1×4 Rx sub-array, denoted as $Rx_{\text{sub},4}(q)$, can be expressed as follows:

$$Rx_{\text{sub},4}(q) = \left[Rx(i,j);\,(i,j) \in S_{q_4}\right], \tag{11}$$

where S_{q_4} represents the set of indices corresponding to the elements in the q^{th} 1×4 Rx sub-array. Fig. 2(b) depicts the mapping of 16 distinct 1×4 sub-arrays for both Tx and Rx. For instance, sub-array 1 for Tx and Rx constitutes antenna elements with index values 1,9,17,25. It can be seen that using 1×4 sub-arrays at Tx and Rx can give rise to $16 \times 16 = 256$ possible combinations for the Tx and Rx sub-array pair selection. Thus, the use of a particular or a fixed Tx and Rx sub-array in FD mMIMO can not suppress the strong SI effectively and limits the potential of utilizing the spatial DoF provided due to the use of large array structures in mMIMO. Hence, finding the optimal Tx and Rx sub-array combination can result in enhanced SI suppression, which can lead to significant performance gains in FD communications.

To further explore the realm of sub-array configurations, we consider the use of 1×8 Tx and Rx sub-arrays. The mapping of the p^{th} 1×8 Tx sub-array, denoted as $Tx_{sub,8}(p)$, can be expressed as follows:

$$Tx_{\text{sub},8}(p) = \left[Tx(i,j);\,(i,j) \in S_{p_8}\right], \tag{12}$$

where S_{p_8} represents the set of indices corresponding to the elements in the p^{th} 1×8 Tx sub-array. Similarly, for the q^{th} 1×8 Rx sub-array, we can write as follows:

$$Rx_{\text{sub},8}(q) = \left[Rx(i,j);\,(i,j) \in S_{q_8}\right], \tag{13}$$

where S_{q_8} represents the set of indices corresponding to the elements in the q^{th} 1×8 sub-array. Fig. 2(c) depicts the mapping for different 1×8 sub-arrays for both Tx and Rx. For instance, sub-array 1 for Tx and Rx now constitutes antennas with indices 1,9,17,25,33,41,49,57. The selection of 1×8 Tx and 1×8 Rx sub-array gives rise to $8 \times 8 = 64$ possible combinations for SAS.

B. PROBLEM FORMULATION

We aim to address a multi-objective optimization framework that involves two primary design objectives: 1) minimizing self-interference; and 2) maximizing achievable rate in FD mMIMO systems. To achieve this, we present a formulation that balances these objectives within a MOOP framework.

Objective 1 - Minimizing Self-Interference: We consider minimizing the strong SI caused by simultaneous transmission and reception in the FD system. We quantify SI by

considering the average power of the interference signal between UL and DL channels. Based on the DL and UL RF beamforming stages, we can express the total achieved SI for FD mMIMO system as follows:

$$\mathrm{A_{SI}} = -10\log_{10}\left(\frac{1}{N}\sum\nolimits_n \left|\mathbf{f}_U^T\left(\hat{\theta}_U\right)\mathbf{H}_{\mathrm{SI}}(:,:,n)\mathbf{f}_D\left(\hat{\theta}_D\right)\right|^2\right). \tag{14}$$

Lemma 1: If $\mathbf{F}_D$ and $\mathbf{F}_U$ are the DL and UL beamforming stages, respectively. Then, for a given $(i,j)^{th}$ DL-UL pair $\{\theta_{D_i}, \theta_{U_j}\}$ in large array structures, the following holds:

$$\mathbf{F}_U\mathbf{H}_{\mathrm{SI}}\mathbf{F}_D \approx \mathbf{0}. \tag{15}$$

Proof: See the Appendix. ■

By steering the UL and DL beams to the desirable directions (i.e., $\hat{\theta}_U = \theta_U$, $\hat{\theta}_D = \theta_D$), we can get maximum directivity in DL and UL directions, which can be given as:

$$|\Phi_D^T(\theta_D)\mathbf{f}_D\left(\hat{\theta}_D\right)|^2 = M_{ds},\ |\mathbf{f}_U^T\left(\hat{\theta}_U\right)\Phi_U(\theta_U)|^2 = M_{us}. \tag{16}$$

For a FD mMIMO system consisting of DL and UL RF beamformers $\mathbf{f}_D$ and $\mathbf{f}_U$, and using sub-array structures at Tx and Rx of BS, the total achieved SI can be minimized by the optimization of UL and DL perturbation angles $\hat{\theta}_U$, $\hat{\theta}_D$ jointly with finding best combination of Tx and Rx sub-arrays. Let p and q represents the sub-array index for Tx and Rx, respectively, then, we can formulate the optimization problem for achieved SI as follows:

$$\begin{aligned}\min_{\left\{\hat{\theta}_D,\hat{\theta}_U,p,q\right\}}\ & \frac{1}{N}\sum\nolimits_n \left|\mathbf{f}_U^T\left(\hat{\theta}_U\right)\mathbf{H}_{\mathrm{SI},p,q}(:,:,n)\mathbf{f}_D\left(\hat{\theta}_D\right)\right|^2 \\ \text{s.t.}\ & C_1\colon M_D - |\Phi_D^T(\theta_D)\mathbf{f}_D\left(\hat{\theta}_D\right)|^2 \le \epsilon, \\ & C_2\colon M_U - |\mathbf{f}_U^T\left(\hat{\theta}_U\right)\Phi_U(\theta_U)|^2 \le \epsilon, \\ & C_3\colon \sum_q x_{pq} = 1\ \forall p, \\ & C_4\colon \sum_p x_{pq} = 1\ \forall q, \end{aligned} \tag{17}$$

where C_1 and C_2 refers to the directivity degradation constraints in DL and UL directions, respectively. In other words, the constraints mean that we limit the degradation of directivities from the main beam directions θ_D and θ_U to a small value ϵ. The constraints C_3 and C_4 ensure that exactly one Tx sub-array is selected for each Rx sub-array and vice versa, resulting in a one-to-one mapping between the Tx and Rx sub-arrays. The optimization problem defined in (17) is non-convex and intractable due to the non-linearity constraints.

Objective 2 - Maximizing Total Achievable Rate: The second objective is to maximize the total achievable data rate in FD system. Using the SINR expressions for both DL and UL (as given in (4) and (6)), we can write the achievable rate for the DL and UL UE as follows:

$$\begin{aligned}\mathrm{R}_D &= \log_2(1+\mathrm{SINR}_D) \\ \mathrm{R}_U &= \log_2(1+\mathrm{SINR}_U) \\ \mathrm{R_T} &= \mathrm{R}_D + \mathrm{R}_U, \end{aligned} \tag{18}$$

where R_D and R_U are the achievable rates for DL and UL UE, respectively. Then, the optimization problem can be expressed as follows:

$$\begin{aligned}\max_{\left\{\hat{\theta}_D,\hat{\theta}_U,p,q\right\}}\ & \mathrm{R_T}\left(\hat{\theta}_D,\hat{\theta}_U,p,q\right) \\ \text{s.t.}\ & C_1 - C_4. \end{aligned} \tag{19}$$

Multi-Objective Optimization Problem: To balance the conflicting objectives of minimizing self-interference and maximizing achievable rate, we formulate a multi-objective optimization problem. We introduce a weighting factor, α, to adjust the trade-off between the objectives. Then, the problem can be expressed as follows:

$$\begin{aligned}\min_{\left\{\hat{\theta}_D,\hat{\theta}_U,p,q\right\}}\ & \frac{1}{N}\sum\nolimits_n \left|\mathbf{f}_U^T\left(\hat{\theta}_U\right)\mathbf{H}_{\mathrm{SI},p,q}(:,:,n)\mathbf{f}_D\left(\hat{\theta}_D\right)\right|^2 - \alpha\mathrm{R_T} \\ \text{s.t.}\ & C_1 - C_4. \end{aligned} \tag{20}$$

In this formulation, the objective combines the minimized SI term with the weighted negative logarithm of the total achievable rate to balance the objectives. By varying the weighting factor α, we can explore different trade-offs between self-interference and achievable rate.[3]

Remark: This problem formulation is tailored to address the objectives of minimizing SI and maximizing total achievable rate in an FD communications system. It accounts for the UL/DL RF beamforming vectors, interference thresholds, and SINR values to guide the optimization process. The multi-objective optimization approach allows for using mMIMO spatial DoF to achieve different trade-offs between the objectives.

Our objective in this research work is to consider the practical FD mMIMO implementation using OTA measured SI channel and to study the capacity gains of FD mMIMO system over HD transmissions using the data-driven analysis. Therefore, the proposed solution can help to understand how close the FD systems can achieve in terms of theoretical doubling of the achievable rate by suppressing strong SI based on beamforming capability of mMIMO systems. Then, the phase response vectors can be written as follows:

$$\boldsymbol{\phi}_D(\theta_D) = \left[1, e^{-j2\pi d\cos(\theta_D)}, \ldots, e^{-j2\pi d(M_{ds}-1)\cos(\theta_D)}\right]^T \in \mathbb{C}^{M_{ds}\times 1}, \tag{21}$$

$$\boldsymbol{\phi}_U(\theta_U) = \left[1, e^{j2\pi d\cos(\theta_U)}, \ldots, e^{j2\pi d(M_{us}-1)\cos(\theta_U)}\right]^T \in \mathbb{C}^{M_{us}\times 1}. \tag{22}$$

IV. PROPOSED HBF WITH SAS

In this section, our objectives are to suppress strong SI and maximize the total achievable rate solely by utilizing the spatial DoF of the large array structures, which can avoid the use of costly analog SI-cancellation circuits. In particular, we use a swarm intelligence-based algorithmic solution

[3]Here, our objective is to enhance FD capacity while suppressing SI. Therefore, the optimization of α is beyond the scope of this paper.

and present the HBF design based on beam perturbations jointly with SAS approach, where the Tx and Rx sub-arrays are selected jointly with perturbed UL and DL RF beam angles to minimize MOOP (as given in (20)) while satisfying the directivity degradation constraints in the respective directions.

A. RF STAGES DESIGN

In the rest of this section, we discuss the proposed HBF with following two schemes: 1) OBF RF beamformer; and 2) NOBF RF beamformer with SAS.

1) OBF RF BEAMFORMER DESIGN

In this scheme, our aim is to suppress the strong SI and maximize R_T via designing the DL RF stage $\mathbf{f}_D$, which steers the beam at DL user jointly with the design of UL RF stage $\mathbf{f}_U$ for UL user. The objective here is to generate the orthogonal beams, which are steered at the desired DL and UL user, which are located at θ_D and θ_U, respectively. In particular, we use the measured SI channel $\mathbf{H}_{\text{SI}}$, which consists of LoS path components. Then, the effective reduced-size SI channel matrix as seen from the BB-stages can be written as follows:

$$\mathcal{H}_{\text{SI}}(:,:,n) = \mathbf{f}_U^T \mathbf{H}_{\text{SI}}(:,:,n)\mathbf{f}_D. \tag{23}$$

Based on the orthogonality principle, we can generate $M_{ds}(M_{us})$ orthogonal DL (UL) beams. Here, the design of DL and UL OBF RF stages, which satisfies the orthogonality property, can be given as follows [35]:

$$\mathbf{f}_D^{\text{OBF}}(\theta_D) = \frac{1}{\sqrt{M_{ds}}}\left[1, e^{j2\pi d\cos(\theta_D)}, \ldots, e^{j2\pi d(M_{ds}-1)\cos(\theta_D)}\right]^T \tag{24}$$

$$\mathbf{f}_U^{\text{OBF}}(\theta_U) = \frac{1}{\sqrt{M_{us}}}\left[1, e^{-j2\pi d\cos(\theta_U)}, \ldots, e^{-j2\pi d(M_{us}-1)\cos(\theta_U)}\right]^T. \tag{25}$$

The use of SC architecture for beamforming simplifies the design of $\mathbf{f}_D^{\text{OBF}}$ and $\mathbf{f}_U^{\text{OBF}}$ as it requires only $\log_2(M_{ds})$ and $\log_2(M_{us})$ PSs at Tx and Rx, respectively when compared to $\log_2(M_D)$ and $\log_2(M_U)$ PSs when using FC antenna array. The OBF RF stages are formulated using the DL/UL angle pair while satisfying CM constraints.

2) NOBF RF BEAMFORMER WITH SAS DESIGN

The simulation results in [35] show that HBF based on NOBF RF beamformer stages can achieve better SI suppression than OBF RF stages, where the latter is formulated using the orthogonal angle pairs. In this proposed HBF scheme using NOBF RF stages, our motivation is to suppress the strong SI while maximizing the total achievable rate for a FD mMIMO system using a measured SI channel (i.e., real-time implementation). Particularly, we introduce beam perturbations jointly with Tx-Rx SAS to design the RF beamforming stages.

Remark 1: The orthogonality constraint limits the number of orthogonal UL and DL beam pairs that can be supported in a given system, which can become a bottleneck in scenarios of high user density. As the number of UL and DL users increases, the available orthogonal resources may be exhausted, leading to reduced system capacity and throughput.

Remark 2: Compared to the NOBF scheme in [35], which introduces phase-range constraint scheme, the proposed directivity-loss constraint NOBF scheme allows a more freedom to perturb the orthogonal beams while keeping the directivity loss to a small value. Moreover, the proposed NOBF scheme in [35] is limited by the quantized angle pairs, where the users' AoD and AoA have to be quantized, and then the DL and UL beams are steered within the boundary of the quantized angles. Thus, for a small number of antennas, the quantization process can introduce large errors, which can result in reduced directivity gain. On the other hand, the quantization error can be low for large number of antennas, however, the non-orthogonal beams can only be steered within tight boundaries, so the beamforming-based SI suppression might be limited.

Remark 2: The use of SC Tx and Rx structures enable the creation of a reduced-size SI channel matrix based on the chosen Tx and Rx sub-array configuration. This reduced-size matrix captures the SI channel characteristics specific to the selected antennas. By leveraging the spatial properties of the sub-arrays, the SI channel exhibits improved isolation and reduced coupling, leading to a lower level of SI. By choosing the best subset of antennas, we can increase the spatial separation between the desired signal and the interfering signals, thereby augmenting the system's capability to support multiple independent spatial channels simultaneously. This increased spatial DoF translates into higher capacity, improved system performance, and efficient management of interference in FD mMIMO systems.

As a continuation to the SI suppression scheme in [35], we propose to explore the HBF with NOBF RF beamformers jointly with SAS to minimize SI and maximize capacity. Instead of using the quantized angle pairs, we allow the DL and UL beams to be slightly steered away from the AoD and AoA angles to minimize the SI power while maintaining possible degradation in directivity within affordable constraints. In particular, the proposed NOBF with SAS approach optimize the UL and DL RF beamformers via new non-orthogonal angles as well as selects the best Tx-Rx sub-array pair for enhanced SI suppression in FD mMIMO systems. For a given orthogonal angle pair $\{\theta_D, \theta_U\}$, we introduce a perturbation to make them non-orthogonal angle pair to suppress SI (i.e., the UL and DL RF beamformers steer the non-orthogonal beams at $\{\hat{\theta}_D, \hat{\theta}_U\}$).

We propose a swarm intelligence inspired particle swarm optimization (PSO)-based perturbation scheme to solve the challenging non-convex optimization problem (as given in (20)), which can find the optimal DL and UL beam directions $\hat{\theta}_D, \hat{\theta}_U$ jointly with Tx and Rx best sub-array pair $\{p, q\}$ to minimize SI and maximize total achievable rate while satisfying the corresponding directivity degradation and SAS constraints $C_1 - C_4$. The algorithm starts with a

swarm of Z particles, each with its own position, velocity, and fitness value, which are randomly placed in optimization search space of perturbation coefficients. During a total of T iterations, the particle z communicates with each other, and move for the exploration of the optimization space to find the optimal solution. Let $\mathbf{X}_z^{(t)}$ be the perturbation vector of z^{th} particle during t^{th} iteration, which consists of optimization variables, and can be given as follows:

$$\mathbf{X}_z^{(t)} = \left[\hat{\theta}_D^z, \hat{\theta}_U^z, p^z, q^z\right], \tag{26}$$

where $z = 1, \ldots, Z$ and $t = 0, 1, \ldots, T$. For each z^{th} particle, by substituting (26) in (24) and (25), the DL and UL NOBF RF beamformers $\mathbf{f}_D(\mathbf{X}_z^{(t)})$ and $\mathbf{f}_U(\mathbf{X}_z^{(t)})$ can be obtained as function of perturbation angles $\hat{\theta}_D^z$ and $\hat{\theta}_U^z$, respectively. By using (14), MOOP can be written as:

$$\frac{1}{N}\sum\nolimits_n \left|\mathbf{f}_U^T\left(\mathbf{X}_z^{(t)}\right)\mathbf{H}_{\mathrm{SI}}\left(\mathbf{X}_z^{(t)}\right)\mathbf{f}_D\left(\mathbf{X}_z^{(t)}\right)\right|^2 - \alpha \mathrm{R}_{\mathrm{T}}\left(\mathbf{X}_z^{(t)}\right) \tag{27}$$

Based on the sub-array mapping as discussed in Section III-A, each z^{th} particle finds the best Tx-Rx sub-array indices p^z, q^z, and uses the corresponding measured SI channel $\mathbf{H}_{\mathrm{SI}}(\mathbf{X}_z^{(t)})$ instead of using the complete measured SI channel $\mathbf{H}_{\mathrm{SI,ALL}}$, which greatly reduces SI. Then, the personal best for the z^{th} particle and the current global best among all particles at the t^{th} iteration, are respectively found as follows

$$\mathbf{X}_{\mathrm{best},z}^{(t)} = \underset{\mathbf{X}_z^{(t^*)}, \forall t^*=0,1,\ldots,t}{\arg\min} \frac{1}{N}\sum\nolimits_n \left|\mathbf{f}_U^T\left(\mathbf{X}_z^{(t)}\right)\mathbf{H}_{\mathrm{SI}}\left(\mathbf{X}_z^{(t)}\right)\mathbf{f}_D\left(\mathbf{X}_z^{(t)}\right)\right|^2 - \alpha \mathrm{R}_{\mathrm{T}}\left(\mathbf{X}_z^{(t)}\right) \tag{28}$$

$$\mathbf{X}_{\mathrm{best}}^{(t)} = \underset{\mathbf{X}_{\mathrm{best},z}^{(t)}, \forall z=0,1,\ldots,Z}{\arg\min} \frac{1}{N}\sum\nolimits_n \left|\mathbf{f}_U^T\left(\mathbf{X}_{\mathrm{best},z}^{(t)}\right)\mathbf{H}_{\mathrm{SI}}\left(\mathbf{X}_{\mathrm{best},z}^{(t)}\right)\mathbf{f}_D\left(\mathbf{X}_{\mathrm{best},z}^{(t)}\right)\right|^2 - \alpha \mathrm{R}_{\mathrm{T}}\left(\mathbf{X}_{\mathrm{best},z}^{(t)}\right) \tag{29}$$

The convergence of the proposed joint NOBF scheme with SAS for enhanced SI suppression depends on the velocity vector $\mathbf{v}_z$ for both personal best $\mathbf{X}_{\mathrm{best},z}$ and global best $\mathbf{X}_{\mathrm{best}}$ solutions, which is defined as follows:

$$\mathbf{v}_z^{(t+1)} = \Omega_1\left(\mathbf{X}_{\mathrm{best}}^{(t)} - \mathbf{X}_z^{(t)}\right) + \Omega_2\left(\mathbf{X}_{\mathrm{best},z}^{(t)} - \mathbf{X}_z^{(t)}\right) + \Omega_3^{(t)} v_z^{(t)}, \tag{30}$$

where $\mathbf{v}_z^{(t)}$ is the velocity of the z^{th} particle at the t^{th} iteration, Ω_1, Ω_2 are the random diagonal matrices with the uniformly distributed entries over $[0, 2]$ and represent the social relations among the particles, and the tendency of a given particle for moving towards its personal best, respectively. Here, $\Omega_3 = (\frac{T-1}{T})\mathbf{I}_{(2N_D+2N_U)}$ is the diagonal inertia weight matrix, which finds the balance between exploration and exploitation for optimal solution in search space. By using (30), the position of each particle during t^{th} iteration is updated as:

$$\mathbf{X}_z^{(t+1)} = \mathrm{clip}\left(\mathbf{X}_z^{(t)} + \mathbf{v}_z^{(t+1)}, \mathbf{X}_{\mathrm{Low}}, \mathbf{X}_{\mathrm{Upp}}\right), \tag{31}$$

where $\mathbf{X}_{\mathrm{Low}} \in \mathbb{R}^{(2N_D+2N_U)}$ and $\mathbf{X}_{\mathrm{Upp}} \in \mathbb{R}^{(2N_D+2N_U)}$ are the lower-bound and upper-bound vectors for the perturbation coefficients, respectively, and are constructed according to the earlier defined boundaries of each perturbation coefficient given in $C_1 - C_4$. Here, we define $\mathrm{clip}(x, a, b) = \min(\max(x, a), b)$ as the clipping function to avoid exceeding the bounds. Furthermore, different from the sub-optimal approach, we here consider each perturbation coefficient as a continuous variable inside its boundary. Then, we can design the NOBF RF stages with SAS as follows:

$$\mathbf{f}_D^{\mathrm{NOBF}}\left(\hat{\theta}_D, p\right) = \frac{1}{\sqrt{M_{ds}^{(p)}}}\left[1, e^{j2\pi d\cos\left(\hat{\theta}_D\right)}, \ldots, e^{j2\pi d\left(M_{ds}^{(p)}-1\right)\cos\left(\hat{\theta}_D\right)}\right]^T \tag{32}$$

$$\mathbf{f}_U^{\mathrm{NOBF}}\left(\hat{\theta}_U, q\right) = \frac{1}{\sqrt{M_{us}^{(q)}}}\left[1, e^{-j2\pi d\cos\left(\hat{\theta}_U\right)}, \ldots, e^{-j2\pi d\left(M_{us}^{(q)}-1\right)\cos\left(\hat{\theta}_U\right)}\right]^T. \tag{33}$$

The design of proposed swarm intelligence-based NOBF RF stages utilizing beam perturbations jointly with SAS is summarized in Algorithm 1.

Algorithm 1: Proposed Swarm Intelligence-Based NOBF RF Stages With SAS

Input: $Z, T, M_{ds}, M_{us}, \mathbf{H}_{SI}, (\theta_D, \psi_D), (\theta_U, \psi_U)$.
Output: $\hat{\theta}_D, \hat{\theta}_U$.
for $t = 0 : T$ **do**
  for $z = 1 : Z$ **do**
    if $t = 0$ **then**
      Initialize the velocity as $\mathbf{v}_z^{(0)} = 0$.
      Initialize $\mathbf{X}_z^{(t)}$ uniformly distributed in $[\mathbf{X}_{\mathrm{Low}}, \mathbf{X}_{\mathrm{Upp}}]$.
    else
      Update the velocity $\mathbf{v}_z^{(t)}$ via (30).
      Update the perturbation $\mathbf{X}_z^{(t)}$ via (31).
    end
    Find the personal best $\mathbf{X}_{\mathrm{best},z}^{(t)}$ via (28).
  end
  Find the global best $\mathbf{X}_{\mathrm{best}}^{(t)}$ as in (30).
  Design RF stages $\mathbf{f}_D$, $\mathbf{f}_U$ via (32),(33).
end

B. BB STAGES DESIGN

After designing the RF beamformers $\mathbf{f}_D$ and $\mathbf{f}_U$, the BB precoder stages $\mathbf{B}_D$ and $\mathbf{B}_U$ only employ the reduced-size effective downlink channel matrix $\boldsymbol{\mathcal{H}}_D = \mathbf{H}_D\mathbf{f}_D \in \mathbb{C}^{K_D \times N_D}$ and uplink channel matrix $\boldsymbol{\mathcal{H}}_U = \mathbf{f}_U\mathbf{H}_U \in \mathbb{C}^{N_U \times K_U}$, respectively. Therefore, it remarkably reduces the channel estimation overhead size in the FD mMIMO systems with large antenna arrays. Considering that the number of RF chains in the proposed FD SC-HBF scheme is significantly smaller than the number of antennas (i.e., $N_D \ll M_{ds}$ and $N_U \ll M_{us}$), the utilization of effective DL/UL channel matrices reduces the total CSI overhead size from $M_{ds} \times K_D + M_{us} \times K_U$ to $N_D \times K_D + N_U \times K_U$. It is important to highlight that the instantaneous SI channel matrix $\mathbf{H}_{\mathrm{SI}}$ is not required in the proposed BB precoder/combiner

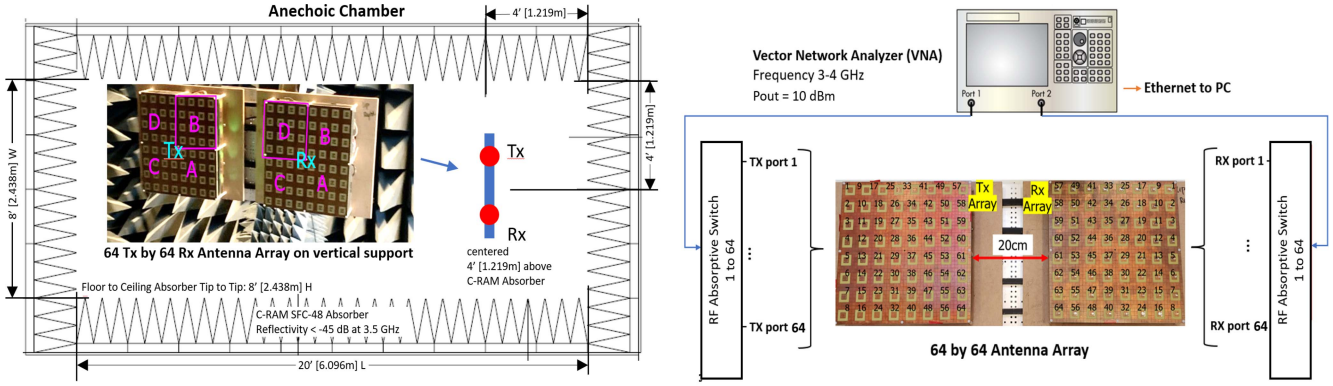

FIGURE 3. OTA FD mMIMO lab setup for SI measurement. (a) Anechoic chamber. (b) Tx and Rx setup.

design. We here develop BB precoder/combiner via applying regularized zero-forcing (RZF). Here, the primary objective is maximizing the intended DL and UL signal power while suppressing the IUI power. According to the well-known RZF technique, we first define the BB DL stage as follows:

$$\mathbf{B}_D = \kappa_D \mathbf{X}_D^{-1} \boldsymbol{\mathcal{H}}_D^H \in \mathbb{C}^{N_D \times K_D} \tag{34}$$

where $\kappa_D = \sqrt{P_D / \operatorname{tr}(\boldsymbol{\mathcal{H}}_D \mathbf{X}_D^{-1} \mathbf{f}_D^H \mathbf{f}_D \mathbf{X}_D^{-1} \boldsymbol{\mathcal{H}}_D^H)}$ is the normalization scalar satisfying the maximum DL transmit power constraint of P_D as indicated in Section II-A. According to the RZF technique, we here define $\mathbf{X}_D = \boldsymbol{\mathcal{H}}_D^H \boldsymbol{\mathcal{H}}_D + \frac{\sigma_w^2}{P_D/K_D} \mathbf{I}_{N_D} \in \mathbb{C}^{N_D \times N_D}$, which aims to eliminate IUI by taking noise power σ_w^2 into account for the regularization. Similarly, the UL BB stage $\mathbf{B}_U$ is also designed as:

$$\mathbf{B}_U = \boldsymbol{\mathcal{H}}_U^H \mathbf{X}_U^{-1} \in \mathbb{C}^{K_U \times N_U}, \tag{35}$$

where $\mathbf{X}_U = \boldsymbol{\mathcal{H}}_U \boldsymbol{\mathcal{H}}_U^H + \frac{\sigma_w^2}{P_U} \mathbf{I}_{N_U} \in \mathbb{C}^{N_U \times N_U}$ according to the RZF technique.

V. ILLUSTRATIVE RESULTS

In this section, we present the Monte Carlo simulation results to illustrate the performance of the proposed HBF with NOBF RF beamformers and SAS scheme in FD mMIMO systems. In particular, we consider the measured SI channel in an anechoic chamber to provide realistic SI suppression capability and capacity gain of a practical FD mMIMO system over HD mMIMO system. We consider $N_D = N_U = 1$ RF chain to serve a single UL and DL UE with 1×4 and 1×8 sub-array configurations for the results presented hereafter. It is important to mention that the proposed HBF scheme requires only 1 RF chain as compared to FDBF, which need 4 or 8 RF chains to support single UL and single DL UE. Thus, the proposed HBF scheme significantly reduces the number of RF chains, especially when the number of served users increases. For PSO, we use the following values: $Z = 20$, $\Omega_1 = \Omega_2 = 2$, and $\Omega_3 = 1.1$.

A. MEASURED SI CHANNEL

We consider a measured SI channel based on the measurement setup designed in an anechoic chamber (i.e., without external surrounding reflections) as shown in Fig. 3. The OTA FD lab setup has following internal dimensions: 1) length = 20 ft (6.096 m); 2) width = 8 ft (2.438 m); and 3) height = 8 ft (2.438 m). This non-reflective space was large enough to place our antenna array under test (measuring 84 cm × 32 cm, W×H) on a positioner, approximately 4 ft away from each of C-RAM SFC-48 absorber covered five walls (reflection < −45 dB at 3.5 GHz). We did not observe significant changes to the measured SI channel when slightly rotating the antenna under test. The antenna arrays consisted of 64 right-hand circular polarization Tx elements and 64 left-hand circular polarization Rx elements. These elements were designed to minimize cross-polarization, and all antenna elements shared a common ground plane. Both the Tx and Rx antenna arrays were arranged in an 8×8 URA configuration, with a spacing of 20 cm between these two arrays, enhancing passive isolation. Fig. 3 illustrates the mapping of the 64 Tx and 64 Rx antenna arrays. The S-parameters were measured with vector network analyzer (VNA) Keysight PNA N5247A, configured with an output power of 10 dBm. To reduce the effect of noise on the expected high isolation measurements, intermediate frequency (IF) BW should be set 300 Hz (resulting in an integrated thermal noise power of -149 dBm), and trace smoothing function was set to 1%, the averaging was turned off. The measurement bandwidth was 1 GHz, from 3 GHz to 4 GHz, with a step size of 625 kHz (resulting in 1601 measurement points). The sweep time for each antenna elements pair was ∼10 sec, thus total measurement time for $64 \times 64 = 4096$ combinations, was expected to be 11.5 hrs.

The Tx and Rx antennas were connected to the VNA via 5m long coaxial cables, and MCL USB-1SP16T-83H RF absorptive switches, with approximate total insertion loss of 12.5 dB, on both the Tx and Rx sides. To construct the full 64×64 s-parameters matrix, the measurements were done using two SP16T RF switches (one for Tx and one for Rx)

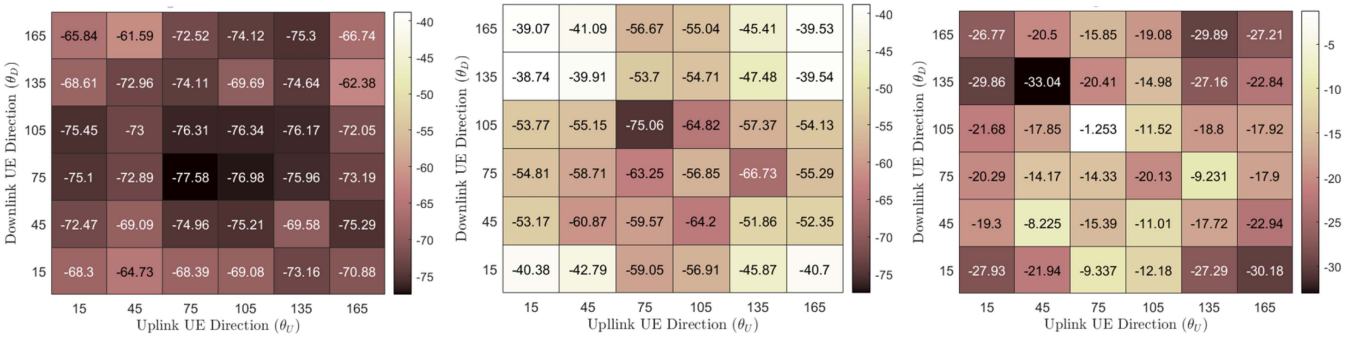

FIGURE 4. Achieved SI suppression using 1×4 sub-array with 20 MHz BW. (a) Proposed NOBF with SAS. (b) OBF. (c) SI suppression gain.

connected to each 4×4 sub-section at a time. The obtained s-parameters were transmitted to a PC via Ethernet and post-processed in MATLAB, to de-embed all insertion losses of the test setup, and to construct 64 Tx by 64 Rx SI channel matrix for further use in analysis and simulations of the FD mMIMO testbed system. The detailed results of the measured 64 Tx by 64 Rx SI channel, such as magnitude, phase, and delay are discussed in detail in [45]. The individual isolation between each Tx and Rx element ranged from approximately 37 dB to 80 dB, thus the resulting minimum SNR, in front of the VNA receiver, was expected to be approximately 54 dB (10dBm – 12.5dB – 80dB – 12.5 dB + 149dBm). The observed trace variations over frequency, for fixed RF attenuator of 100dB at VNA ports, were approximately ±0.75 dB, ±3°, and ±100ps for group delay. This setup is used for SI channel measurement.

The resulting parameters in the form of.S2P file are used to get a 64x64 SI channel matrix, which is mainly due to *internal* coupling between Tx and Rx antenna elements (i.e., consisting of only LoS path components). Then, the complete SI channel matrix $\mathbf{H}_{\text{SI, ALL}}$ has dimensions of 64 × 64 × 1601 for a total of 1601 different frequency points. As mentioned earlier, we consider a ULA sub-array configurations of 4 and 8 antenna elements for both Tx and Rx. Hence, the corresponding SI channels for 1×4 and 1×8 sub-array configurations can be represented as $\mathbf{H}_{\text{SI}} \in \mathbb{C}^{4\times4\times1601}$ and $\mathbf{H}_{\text{SI}} \in \mathbb{C}^{8\times8\times1601}$, respectively. As per 3GPP specification, the UL and DL channel BW can vary from 5 MHz to 100 MHz [46], then the corresponding SI channel for the given BW can be written as: $\mathbf{H}_{\text{SI},B} = \mathbf{H}_{\text{SI}}(:,:,n) \in \mathbb{C}^{i\times i\times n}$, where $i = \{4, 8\}$, B is the given BW, and $n = 1, 2, \ldots, N$ is the sample frequency point for a total of N frequency points in a given BW. For instance, for a BW of 20 MHz, $n = 1, 2, \ldots, 33$ for the frequency range from 3.49 GHz to 3.51 GHz. Similarly, for a BW of 100 MHz, $n = 1, 2, \ldots, 161$ for the frequency range from 3.45 GHz to 3.55 GHz.

B. SELF-INTERFERENCE SUPPRESSION

In this subsection, we first present the results of achieved SI using the proposed HBF scheme for NOBF RF beamformers with SAS, and compare it to HBF scheme with OBF RF beamformer. In Fig. 4, we consider six different angular UE locations (i.e., $\{\theta_D, \theta_U\} \in \{15°{:}30°{:}180°\}$) and generate the results using 1×4 sub-arrays for Tx and Rx antenna elements with a maximum directivity degradation ϵ =1 dB and a bandwidth of 20 MHz. In OBF scheme, the beams generated by the UL and DL RF beamformers are steered at exact UE locations (i.e., both $\mathbf{f}_D(\theta_D)$ and $\mathbf{f}_U(\theta_U)$ steer the beams at θ_D and θ_U, respectively). It can be seen that the design of RF beamformers $\mathbf{f}_D(\theta_D)$ and $\mathbf{f}_U(\theta_U)$ using OBF can achieve SI suppression ranging from -38.74 dB to -75.05 dB for different UL/DL UE angle pairs. On the other hand, the proposed NOBF scheme with SAS can achieve SI suppression ranging from -61.59 dB to -77.57 dB. This shows that the design of RF beamformers $\mathbf{f}_D(\hat{\theta}_D)$, $\mathbf{f}_U(\hat{\theta}_U)$ using the proposed NOBF RF beamformers with SAS can provide an additional SI suppression gain of 19 dB on average when compared to OBF, and can further reduce SI by a maximum of 33.04 dB (e.g., for $\theta_D = 135°, \theta_U = 45°$, SI suppression improves from -39.91 dB to -72.96 dB). In other words, by introducing beam perturbation in both UL and DL directions and the selection of the best Tx-Rx sub-array pair can improve SI suppression capability by more than 82% using the proposed NOBF with SAS HBF scheme.

The use of a larger sub-array at Tx and Rx can generate narrower beams and can serve large number of users. In Fig. 5, we compare the achieved SI suppression results using 1×8 sub-array for six different UL and DL UE angular locations and compare the performance of HBF scheme with NOBF and SAS versus HBF scheme with OBF RF beamformers. It is noteworthy to mention that, even though using a larger array structure can narrow the mainbeam width, however, due to the orthogonality, there is still a limitation on the number of orthogonal UL/DL beams that can be generated with such large array structures. As a result, using OBF restricts the maximum number of UL and DL users that can be served simultaneously in FD mMIMO systems. The proposed HBF with NOBF RF beamformers and SAS can achieve SI suppression ranging between −51.93 dB and −77.45 dB, where the achieved SI suppression for OBF RF beamformers varies between

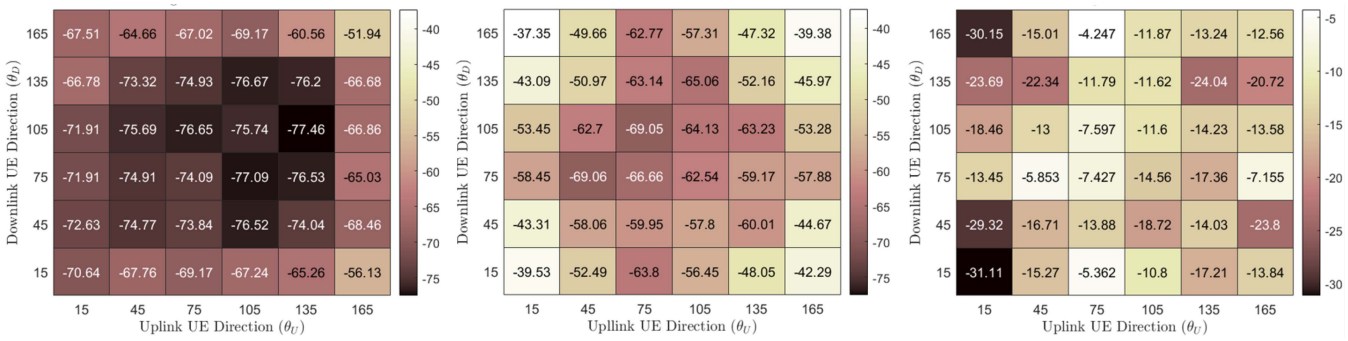

FIGURE 5. Achieved SI suppression using 1×8 sub-array with 20 MHz BW. (a) Proposed NOBF with SAS. (b) OBF. (c) SI suppression gain.

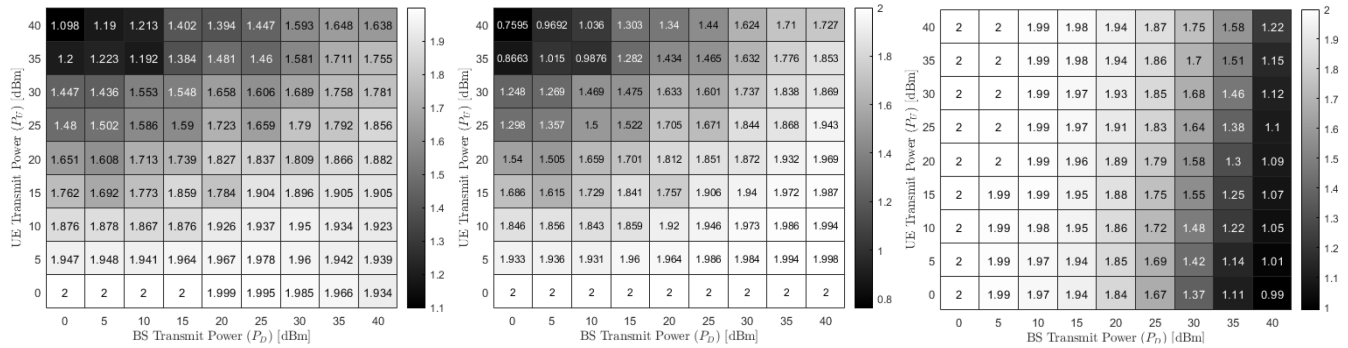

FIGURE 6. FD-to-HD rate ratio versus BS/UE transmit power using OBF with 1 × 4 sub-array at 20 MHz. (a) Total. (b) DL. (c) UL.

−37.35 dB to −69.05 dB. Thus, the proposed HBF scheme with NOBF RF stages and SAS can provide an additional SI suppression gain of around 15.43 dB (on average) with a maximum SI suppression improvement of around -31.11 dB, which represents an enhanced SI suppression capability of 78.69%.

C. FD-TO-HD ACHIEVABLE RATE RATIO

In this subsection, we compare the achievable rate of FD mMIMO system versus the HD mMIMO system for UL and DL transmission. In particular, the UL and DL transmissions are operated separately in the case of HD communications, where the received DL signal given in (3) does not include IUI by UL UE. Similarly, the received UL signal given in (5) does not experience the strong SI. As a benchmark scheme, we consider the angular-based HBF technique in [24], which considers the DL transmission via applying OBF at the RF-stage and RZF at the BB-stage. Similarly, for the UL transmission, we develop the angular-based HC technique using [24] to compare both HD UL and DL rate with FD rate of the proposed HBF scheme. Since the HD DL and UL transmissions are carried out over either different time-slots or different frequency bands, therefore, the DL, UL and total achievable rate in the HD transmission are normalized as: $R_{D,\mathrm{HD}} = \frac{1}{2}R_D$, $R_{U,\mathrm{HD}} = \frac{1}{2}R_U$, and $R_{\mathrm{Total,\,HD}} = R_{D,\mathrm{HD}} + R_{U,\mathrm{HD}}$ respectively. To better compare the achievable rate of FD and HD transmission, we use the FD-to-HD rate ratio, which is defined as $\mathrm{Ratio}_D = \frac{R_{D,\mathrm{FD}}}{R_{D,\mathrm{HD}}}$, $\mathrm{Ratio}_U = \frac{R_{U,\mathrm{FD}}}{R_{U,\mathrm{HD}}}$, and $\mathrm{Ratio}_T = \frac{R_{T,\mathrm{FD}}}{R_{T,\mathrm{HD}}}$, where $R_{D,\mathrm{FD}}$, $R_{U,\mathrm{FD}}$ and $R_{T,\mathrm{FD}}$ are the DL, UL and total achievable rates in FD communications and can be calculated using (18). In Fig. 6, we compare the DL, UL and total FD-to-HD rate ratio versus BS transmit power P_D and UL UE transmit power P_U using the measured SI channel. Given the maximum BS transmit power as 44 dBm at sub−6 GHz band [47], the BS transmit power range is considered as $P_D \in [0, 40]$ dBm. For simplicity, we consider the same range for the UL UE transmit power (i.e., $P_U \in [0, 40]$ dBm) though BS and UE have different hardware constraints. Here, we depict the results for the proposed HBF scheme using OBF RF beamformers to compare the FD-to-HD performance at different BS and UE power levels and to provide understanding of how different power levels can impact the FD achievable rate at a fixed angular location (i.e., $\theta_D = 135°, \theta_U = 15°$).

In Fig. 6(a), the total rate ratio is analyzed, which shows that FD transmission can double the capacity with respect to the conventional HD transmission at low power levels of BS and UL UE. Though the FD-to-HD total rate ratio (Ratio_T) decays for very high UL UE transmit power, the proposed HBF scheme can still provide higher capacity ($\geq R_{T,\mathrm{HD}}$) even for the extreme case of very high UL UE power (i.e., at $P_U = 40$ dBm, $\mathrm{Ratio}_T > 1.0$). As shown in Fig. 6(b),

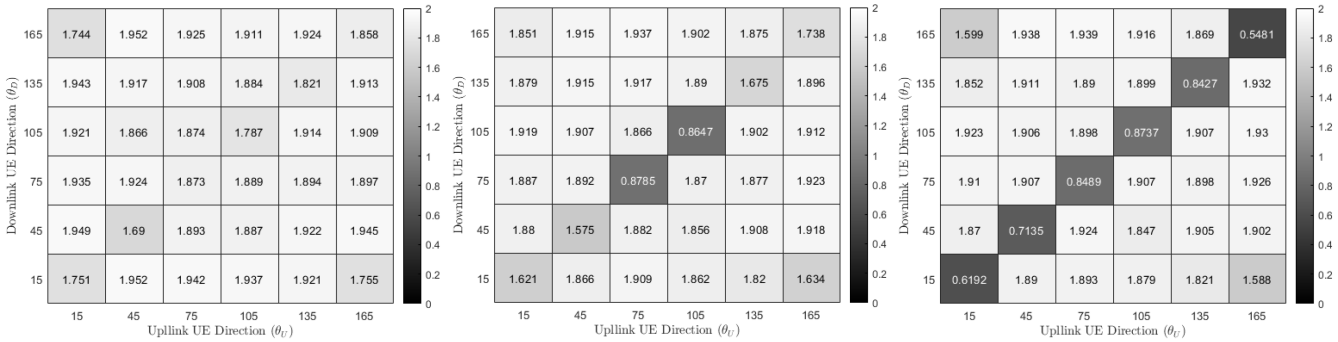

FIGURE 7. FD-to-HD total rate ratio at different UL/DL UE angular locations with 1 × 8 sub-array at 20 MHz. (a) NOBF with SAS. (b) NOBF. (c) OBF.

the DL rate ratio improves when P_D increases and only drops below the unity ratio for $P_U \geq 35$ dBm and low P_D values (i.e., for $P_D \in [0, 10]$ dBm, $\text{Ratio}_T \in [0.8, 1]$. This means HD transmissions can provide higher capacity than FD communications in such cases), where the large UL power boosts the IUI power in comparison to the low DL intended signal power (please see (3)). Similarly, the UL rate ratio as depicted in Fig. 6(c) shows that the increased SI power due to the high BS transmit power negatively affect the UL transmission. For instance, at $P_U = 30$ dBm, the FD-to-HD uplink rate ratio (Ratio_U) is exactly 2.00 and 1.12 for $P_D = 0$ dBm and $P_D = 40$ dBm, respectively.

Fig. 7 depicts the FD-to-HD total rate ratio (Ratio_T) for a fixed BS and UL UE transmit power (i.e., $P_D = 30$ dBm and $P_U = 20$ dBm).[4] Here, we consider six different angular locations for the DL and UL UE (i.e., $\{\theta_D^{\text{ALL}}, \theta_U^{\text{ALL}}\} \in \{15°{:}30°{:}180°\}$) and compares Ratio_T using 1×8 sub-arrays with 20 MHz BW and maximum directivity degradation ϵ =1 dB for the following three cases: 1) Proposed HBF with NOBF RF beamformers with SAS (MOOP); 2) Proposed HBF with NOBF RF beamformers (SOOP)[5]; and 3) Proposed HBF with OBF RF beamformers. Fig. 7 shows that HBF with OBF scheme results in poor FD-to-HD rate ratio when both UL and DL UE have same angular locations (on average the total rate ratio is around 0.74). By using the HBF with NOBF RF stages (SOOP) can significantly increase the rate ratio at most angular locations, however, due to SI channel characteristics and the use of a fixed Tx-Rx sub-array pair, we can see that SOOP can still result in low FD total rate at few angular locations (e.g., $\{\theta_D, \theta_U\} = \{75°, 105°\}$, and HD transmissions can provide better total rate than FD communications at these angular locations). Moreover, the use of a larger sub-array can still suffer from low FD-to-HD total ratio at certain angular locations, and the number of such angle pairs with low FD-to-HD rate ratio can increase for even larger array structures. This issue can be resolved by using HBF with NOBF RF beamformer jointly with SAS, which can provide spatial DoF to improve FD rate at all UL/DL UE angular locations. In Fig. 7(a), we can see the mean total FD-to-HD rate ratio is around 1.88 $\{\theta_D^{\text{ALL}}, \theta_U^{\text{ALL}}\}$ and 1.79 $\{\theta_D^{\text{SAME}}, \theta_U^{\text{SAME}}\}$, which represents an increase of around 11.6% and 142.3%, respectively when compared to OBF total rate ratio.

[4]From Fig. 6, we can see that high values of BS and UL UE transmit power can significantly reduce Ratio_T for OBF scheme. Our motivation is to show that using the proposed HBF with NOBF and SAS scheme, we can enhance the total rate in FD communications even for the extreme case of very high power UL UE values, thus achieving Ratio_T close to 2.

[5]In this approach, we design NOBF RF beamformers for single objective optimization problem (i.e., to minimizing SI). We consider fixed Tx-Rx sub-arrays (without SAS) and find the optimal beam perturbations only.

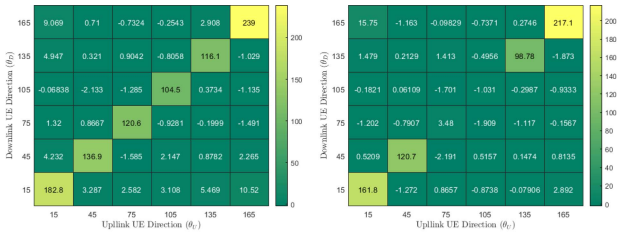

FIGURE 8. FD-to-HD total rate ratio improvement with 1 × 8 sub-array at 20 MHz. (a) NOBF with SAS. (b) NOBF.

Fig. 8 plots the FD-to-HD total rate ratio improvement using 1×8 sub-array. Fig. 8(b) shows the percentage gain in FD-to-HD total rate ratio for the proposed HBF with NOBF RF stages (SOOP) over OBF. We define the percentage improvement in FD-to-HD total rate ratio as follows:

$$\text{Ratio Gain}(\%) = \left(\frac{\text{Ratio}_{T,s} - \text{Ratio}_{OBF}}{\text{Ratio}_{OBF}}\right) \times 100, \quad (36)$$

where s = {NOBF (SOOP), NOBF with SAS (MOOP)}. We can see from Fig. 8 that compared to the mean gains of 6.57% for $\{\theta_D^{\text{ALL}}, \theta_U^{\text{ALL}}\}$ and 87.8% for $\{\theta_D^{\text{SAME}}, \theta_U^{\text{SAME}}\}$ with SOOP, MOOP can provide the mean gains of 11.6% for $\{\theta_D^{\text{ALL}}, \theta_U^{\text{ALL}}\}$ and 142.3% for $\{\theta_D^{\text{SAME}}, \theta_U^{\text{SAME}}\}$.

In Fig. 9, we present the FD-to-HD total rate ratio versus the angular spacing between both UL and DL UE for a fixed power levels using 1×4 sub-array. Here, we consider the DL UE is located at fixed $\theta_D = 75°$ and the UL UE varies its angular location (i.e., $\theta_U \in \{75°{:}1°{:}135°\}$). Thus, the angle separation between UL/DL UE can vary from 0° to 60°. It can be seen that by using the proposed

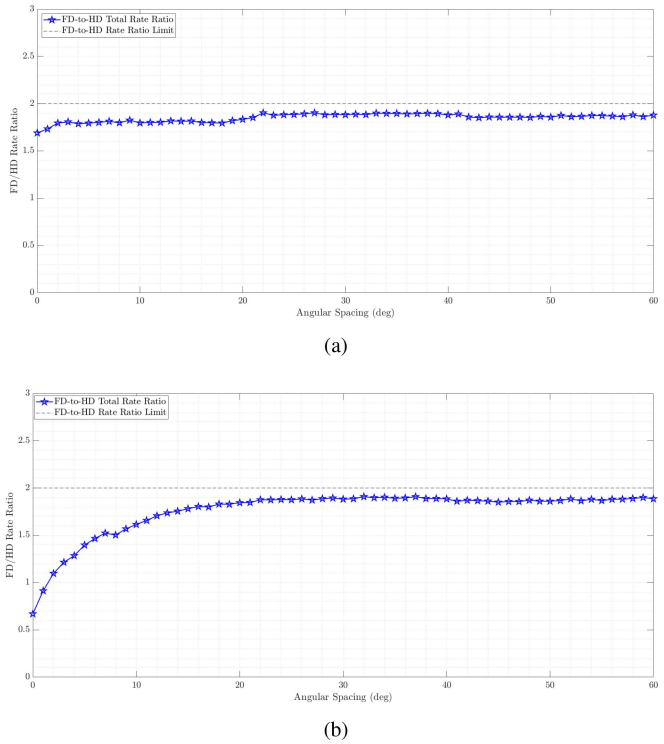

FIGURE 9. FD-to-HD total rate ratio versus angular separation with 1 × 4 sub-array at 20 MHz. (a) NOBF with SAS. (b) OBF.

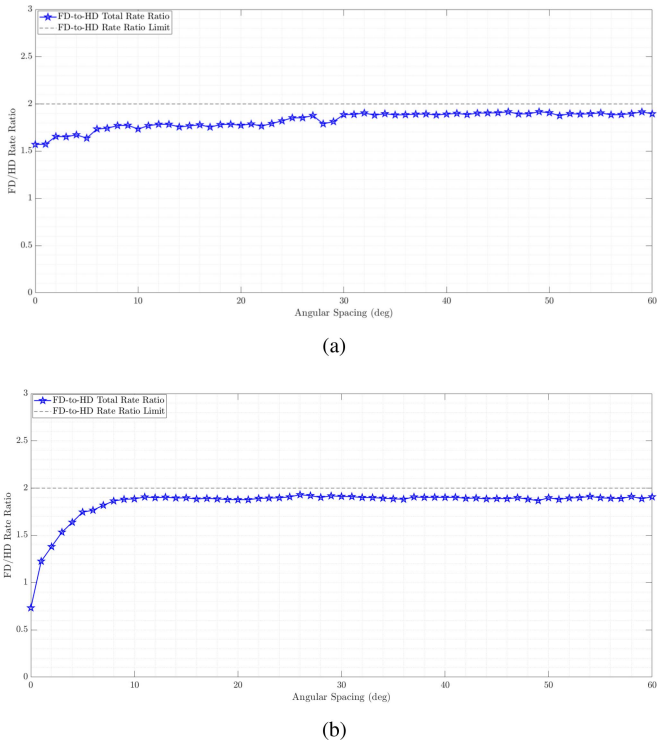

FIGURE 10. FD-to-HD total rate ratio versus angular separation with 1 × 8 sub-array at 20 MHz. (a) NOBF with SAS. (b) OBF.

HBF with NOBF RF stages jointly with SAS (MOOP) can achieve FD-to-HD total rate ratio $\geq$ 1.5 with minimum angle separation of 0°. In other words, the proposed NOBF with SAS (MOOP) can give at least 1.5 times the total achievable rate of HD transmissions irrespective of UL and DL UE locations in FD mMIMO systems, whereas, with OBF scheme, a minimum angle separation of 7° is required to achieve the rate ratio of at least 1.5. For Ratio$_T \geq$ 1.8, we need angle separation of at least 14° with OBF scheme. However, with the proposed NOBF scheme, we require a minimum angle separation of 3°. Similarly, Fig. 10 compares the minimum angle separation for the case when both Tx and Rx are equipped with 1×8 sub-array for DL UE located at fixed $\theta_D = 15°$ and the UL UE varies its angular location (i.e., $\theta_U \in \{15°{:}1°{:}75°\}$). Compared to the minimum angle separation of 3° and 6° for OBF scheme to achieve ratio $\geq$ 1.5 and 1.8, respectively, the proposed HBF scheme with NOBF RF beamformers and SAS (MOOP) scheme only requires 0° and 5° of UL/DL UE angular separation. It must be noted that the use of larger sub-array can generate narrow beams for UL and DL UE, which can reduce IUI, and thus reducing minimum angle separation. In Fig. 11, we compare the total achievable rate versus transmit power of our proposed schemes (i.e., NOBF with SAS (MOOP) and NOBF (SOOP)) with OBF as well as the HBF solutions presented in [22], [23], [33]. We consider $K_D = K_U = 1$, which are located at azimuth angle $\theta_D = 75°, \theta_U = 135°$. By using 1 × 4 Tx and Rx sub-arrays, it can be seen that

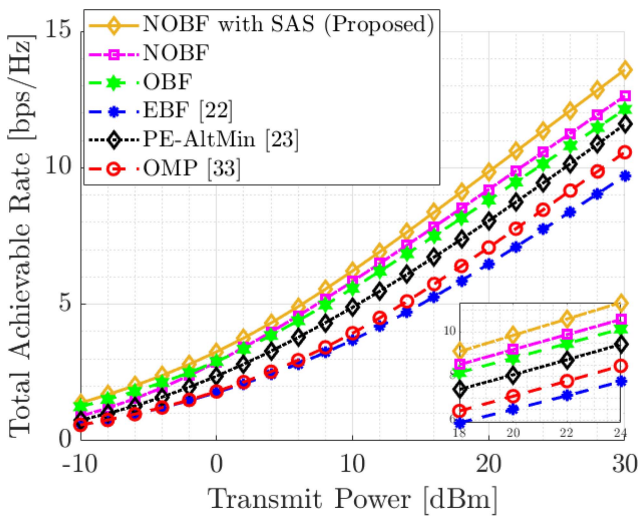

FIGURE 11. Total achievable rate versus transmit power with 1 × 4 sub-array.

compared to OBF and HBF solutions in [22], [23], [33], the proposed NOBF schemes can significantly increase the total achievable rate by suppressing the strong SI. For example, NOBF can provide an increase of 1-2 bps/Hz when compared to OBF, however, by using the proposed NOBF with SAS, we can achieve a gain of around 3-4 bps/Hz. It is noteworthy to mention that our proposed NOBF with SAS can significantly increase the total achievable rate, especially when operating under the following conditions: 1) harnessing a larger sub-array (i.e., 1 × 8); and 2) accommodating a greater number

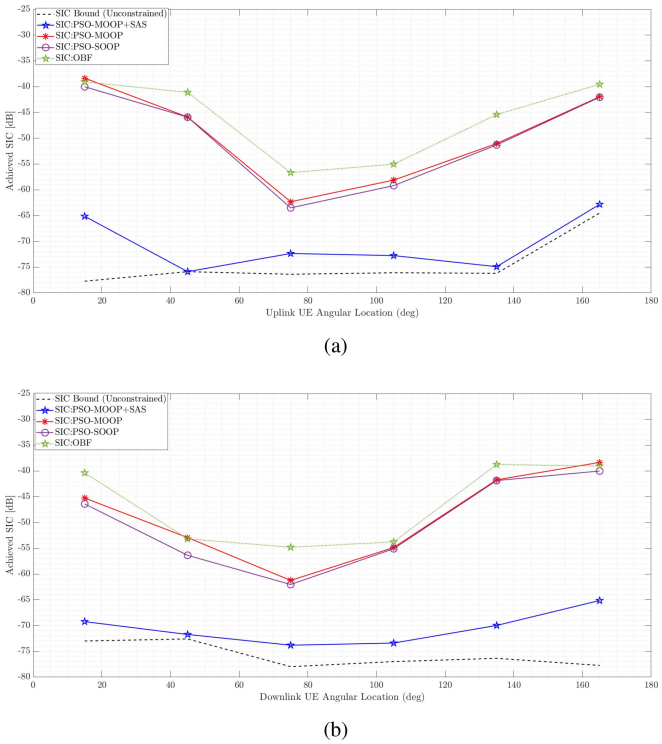

FIGURE 12. SI suppression bound comparison using 1×8 sub-array. (a) Achieved SI versus θ_U. (b) Achieved SI versus θ_D.

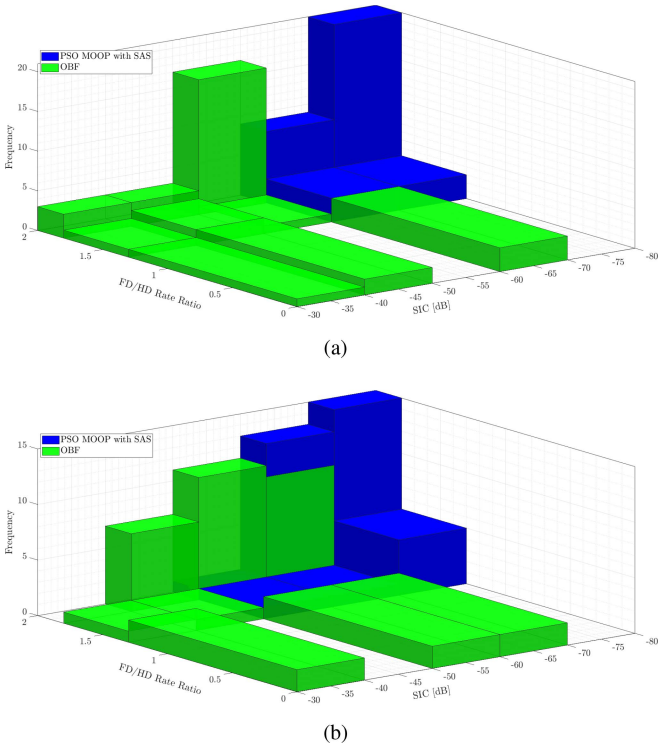

FIGURE 13. Achieved SI and FD-to-HD total rate ratio tradeoff using OBF and NOBF with SAS schemes. (a) 1×4 sub-array. (b) 1×8 sub-array.

of users. This highlights the scalability and adaptability of our approach, offering promising performance enhancements in FD mMIMO systems.

D. CONSTRAINED VERSUS UNCONSTRAINED SI SUPPRESSION COMPARISON

In this section, we compare the achieved SI using 1×8 sub-array for the following schemes: 1) HBF with OBF RF beamformers; 2) HBF with NOBF RF beamformers (NOBF-SOOP); 3) HBF with NOBF RF beamformers (NOBF-MOOP); and 4) HBF with NOBF RF beamformers jointly with SAS (NOBF-MOOP-SAS). For the NOBF schemes, we compare the results for directivity degradation of $\epsilon = 1$ dB. In Fig. 12(a), we plot the achieved SI versus different UL UE angular locations (i.e., $\theta_U \in \{15°{:}30°{:}180°\}$) for a fixed DL UE location ($\theta_D = 165°$). The results show that OBF scheme can provide very low SI suppression with a minimum value of around -55 dB. In comparison, both NOBF schemes (NOBF-SOOP and NOBF-MOOP) can achieve better SI suppression levels at all UL-DL UE angle pairs with a minimum SI suppression of around -63 dB. However, the use of SAS jointly with NOBF for MOOP (NOBF-MOOP-SAS) can reduce SI as low as -76 dB, which is very close to lower bound values of SI suppression. Here, the lower bound for SI suppression level can be achieved by considering the loose directivity degradation limits (i.e., $\epsilon = \infty$). In other words, this loose bound can be considered as an unconstrained optimization, which can allow beam perturbations in both UL and DL directions with high directivity degradation. Our objective here is to show that by using the proposed NOBF-MOOP-SAS with a tight bound of $\epsilon = 1$ dB, we can closely approach the unbounded SI suppression ($\epsilon = \infty$). Compared to the mean difference of 28.3 dB, 24.1 dB of OBF and NOBF-SOOP (NOBF-MOOP) schemes from the lower bound, NOBF-MOOP-SAS has a mean difference of only around 3.81 dB. Similarly, Fig. 12(b) depicts the bounded versus unbounded SI suppression comparisons for different DL UE angular locations (i.e., $\theta_D \in \{15°{:}30°{:}180°\}$) for a fixed UL UE location ($\theta_U = 15°$). Here, we can see that NOBF-MOOP-SAS scheme can achieve SI suppression level close to the bound with an average difference of around 5.2 dB. Thus, we can see that $\mathrm{A}_{\mathrm{SI,NOBF\text{-}MOOP\text{-}SAS}}(\epsilon = \infty) \simeq \mathrm{A}_{\mathrm{SI,NOBF\text{-}MOOP\text{-}SAS}}(\epsilon = 1) \ll \mathrm{A}_{\mathrm{SI,NOBF\text{-}SOOP}}(\mathrm{A}_{\mathrm{SI,NOBF\text{-}MOOP}}) \leq \mathrm{A}_{\mathrm{SI,OBF}}$.

E. ACHIEVED SI AND ACHIEVABLE RATE RATIO TRADEOFF

In this section, we compare the achieved SI as well as FD-to-HD total rate ratio for six different UL and DL locations (i.e., $\{\theta_D, \theta_U\} \in \{15°{:}30°{:}180°\}$), which generates 36 possible UL-DL angle pairs. Fig. 13(a) evaluates the frequency (number of occurrences) of UL-DL angle pairs while satisfying certain performance metric. For instance, using OBF scheme, we

TABLE 1. Performance comparison: NOBF with SAS vs. OBF (1×4 and 20 MHz BW).

Performance Metrics		HBF Scheme			Improvement using NOBF HBF	
		OBF	NOBF			
			SOOP	MOOP with SAS	SOOP vs. OBF	MOOP + SAS vs. OBF
Achieved SI(dB)	Best[6]	-75.05	-75.9	-77.57	16.25	33.04
	Worst	-38.74	-40.01	-61.59	0.569	1.25
	Avg	-52.6	-59.69	-71.96	7.07	19.33
FD-to-HD Total Rate Ratio (All UL/DL UE locations) $[15° : 30° : 165°]$	Best	1.930	1.929	1.948	225.8	261.1
	Worst	0.514	0.597	1.598	-6.18	-5.887
	Avg	1.650	1.780	1.886	7.87	14.3
FD-to-HD Total Rate Ratio (Same UL/DL UE locations) $[15° : 30° : 165°]$	Best	0.879	1.674	1.885	225.8	261.1
	Worst	0.514	0.597	1.598	1.56	83.51
	Avg	0.730	1.371	1.774	87.6	143

TABLE 2. Performance comparison: NOBF with SAS vs. OBF (1×8 and 20 MHz BW).

Performance Metrics		HBF Scheme			Improvement using NOBF HBF	
		OBF	NOBF			
			SOOP	MOOP with SAS	SOOP vs. OBF	MOOP + SAS vs. OBF
Achieved SI(dB)	Best	-69.0	-77.46	-77.45	17.3	31.11
	Worst	-37.35	-38.9	-51.93	1.16	4.24
	Avg	-55.0	-62.59	-70.43	7.58	15.43
FD-to-HD Total Rate Ratio (All UL/DL UE locations) $[15° : 30° : 165°]$	Best	1.939	1.936	1.952	217.1	239
	Worst	0.5481	0.864	1.694	-2.19	-2.13
	Avg	1.689	1.80	1.886	6.57	11.6
FD-to-HD Total Rate Ratio (Same UL/DL UE locations) $[15° : 30° : 165°]$	Best	0.873	1.738	1.872	217.1	239
	Worst	0.548	0.864	1.69	-1.03	104.5
	Avg	0.741	1.392	1.796	87.8	142.3

can achieve SI suppression < -50 dB together with FD-to-HD total rate ratio > 1.5 for a total of $\frac{21}{36}$ UL-DL angle pairs, which represents 58.3% of the total available angle pairs. However, there is $\frac{1}{36}$ UL-DL angle pair to achieve SI < -70 dB jointly with rate ratio > 1.5. On the other hand, the proposed NOBF-MOOP-SAS scheme can provide $\frac{34}{36}$ and $\frac{23}{36}$ UL-DL angle pairs for (achieved SI < -50 dB & Ratio > 1.5) and (achieved SI < -70 dB & Ratio > 1.5), respectively. Similarly, Fig. 13(b) depicts the performance tradeoff using 1×8 sub-array. The OBF scheme results in $\frac{0}{36}$ UL-DL angle pairs to achieve SI < -70 dB & Ratio > 1.5, whereas, the proposed NOBF-MOOP-SAS scheme can provide $\frac{20}{36}$ UL-DL angle pairs to achieve SI < -70 dB & Ratio > 1.5. Thus, the proposed NOBF-MOOP-SAS scheme can achieve high SI suppression jointly with increased FD-to-HD rate ratio for 55% of the UL-DL angle pairs as compared to 0% in the case of OBF scheme. The detailed performance comparison of the proposed NOBF schemes versus OBF for 1×4 and 1×8 sub-array is summarized in Table 1 and Table 2, respectively.[6]

[6]Best or worst improvement is calculated by comparing the angular location of the same uplink and downlink UE pair in both OBF and NOBF schemes.

VI. CONCLUSION

This paper considers a FD mMIMO system using a sub-array-based HBF architecture and investigates the capacity gains of FD communications over HD transmissions in a real-time implementation. In particular, the strong SI is suppressed by designing the RF beamformers jointly with SAS to utilize the spatial DoF in large array structures, thus avoiding the use of costly analog SI-cancellation circuits. To achieve capacity gains in FD communications, a multi-objective design framework is considered to minimize SI and maximize the total achievable rate. Based on OTA measured SI channel, we have proposed a novel HBF scheme that applies perturbations to the orthogonal beams in UL and DL beam directions and jointly finds the best Tx-Rx sub-array pair. To solve this challenging non-convex problem, we have proposed a swarm intelligence-based algorithmic solution to find the optimal perturbations and Tx-Rx indices while satisfying the directivity degradation constraints for the UL and DL beams. Illustrative results show that the proposed HBF scheme with NOBF RF stages jointly with SAS can achieve high SI suppression compared to OBF for both 1×4 and 1×8 sub-array configurations and can mitigate SI to -78 dB in real life implementations for FD mMIMO systems. Moreover, the proposed HBF scheme can achieve an average capacity gain of around 1.8 for any angular location of UL-DL UE.

APPENDIX
PROOF OF LEMMA 1

Let $\mathbf{f}_U$ and $\mathbf{f}_D$ be the UL and DL RF beamformers for i^{th} DL UE and j^{th} UL UE, respectively. Then, we can express the RF beamformers as:

$$\mathbf{f}_D(\theta_{D_i}) = \frac{1}{\sqrt{M_D}}\left[1, e^{j2\pi\Delta\cos(\theta_{D_i})}, \ldots, e^{j2\pi\Delta(M_D-1)\cos(\theta_{D_i})}\right]^T, \quad (37)$$

$$\mathbf{f}_U(\theta_{U_j}) = \frac{1}{\sqrt{M_U}}\left[1, e^{-j2\pi\Delta\cos\left(\theta_{U_j}\right)}, \ldots, e^{-j2\pi\Delta(M_U-1)\cos\left(\theta_{U_j}\right)}\right]^T. \quad (38)$$

Then, we can rewrite the expression for $\mathbf{f}_U^T\mathbf{H}_{SI}\mathbf{f}_D$ as:

$$\begin{aligned}
&\mathbf{f}_U^T\mathbf{H}_{SI}\mathbf{f}_D \\
&= \frac{1}{\sqrt{M_D}}\mathbf{f}_U^T\mathbf{H}_{SI}\left[1, e^{j2\pi d\cos(\theta_{D_i})}, \ldots, e^{j2\pi d(M_D-1)\cos(\theta_{D_i})}\right]^T \\
&= \frac{1}{\sqrt{M_U}}\left[1, e^{-j2\pi d\cos\left(\theta_{U_j}\right)}, \ldots, e^{-j2\pi d(M_U-1)\cos\left(\theta_{U_j}\right)}\right]\mathbf{H}_{SI} \\
&\quad \frac{1}{\sqrt{M_D}}\left[1, e^{j2\pi d\cos(\theta_{D_i})}, \ldots, e^{j2\pi d(M_D-1)\cos(\theta_{D_i})}\right]^T \\
&= \frac{1}{\sqrt{M_D M_U}}\sum_{m_u=1}^{M_U}\sum_{m_d=1}^{M_D} h_{m_u,m_d}e^{-j2\pi d\left(m_u\cos(\theta_{U_j})-m_d\cos(\theta_{D_i})\right)},
\end{aligned} \quad (39)$$

where h_{m_u,m_d} is the (m_u, m_d)-th element of $\mathbf{H}_{SI}$. Since $|\cos(\theta_{U_j})|, |\cos(\theta_{D_i})| \leq 1$, the term inside the exponent of (39) is bounded as follows:

$$\begin{aligned}
&|m_u\cos\left(\theta_{U_j}\right) - m_d\cos\left(\theta_{D_i}\right)| \leq m_u|\cos\left(\theta_{U_j}\right)| + m_d|\cos\left(\theta_{D_i}\right)| \\
&\leq m_u + m_d \leq M_{us} + M_{ds} - 2,
\end{aligned} \quad (40)$$

where the last inequality follows because m_u and m_d both range from 1 to M_U and M_D, respectively. Now, let us consider the term h_{m_u,m_d}. Considering the large array structures, the path loss between the transmit and receive antennas within the same device is generally low due to the short distance between them. Thus, the SI channel, which is the channel from the transmit antenna to the receive antenna in the same device, is expected to be very strong in magnitude. Hence, we can assume that h_{m_u,m_d} has non-negligible values. Next, we analyze the magnitude of the expression $\mathbf{f}_U^T\mathbf{H}_{SI}\mathbf{f}_D$. Applying the triangle inequality, we can write as follows:

$$\begin{aligned}
&|\mathbf{f}_U^T\mathbf{H}_{SI}\mathbf{f}_D| \\
&= \frac{1}{\sqrt{M_D M_U}}\left|\sum_{m_u=1}^{M_U}\sum_{m_d=1}^{M_D} h_{m_u,m_d}e^{-j2\pi d\left(m_u\cos(\theta_{U_j})-m_d\cos(\theta_{D_i})\right)}\right| \\
&\leq \frac{1}{\sqrt{M_D M_U}}\sum_{m_u=1}^{M_U}\sum_{m_d=1}^{M_D}|h_{m_u,m_d}| \\
&\leq \frac{1}{\sqrt{M_D M_U}}(M_U + M_D - 2)\max_{m_u,m_d}|h_{m_u,m_d}|,
\end{aligned} \quad (41)$$

where the last inequality holds due to the bounds on the indices m_u and m_d. Based on the assumption that the path loss is significant and the SI channel is strong, we can infer that the maximum absolute value of the SI channel coefficients $\max_{m_u,m_d}|h_{m_u,m_d}|$ is very small. Consequently, we can approximate the expression as follows:

$$|\mathbf{f}_U^T\mathbf{H}_{SI}\mathbf{f}_D| \approx \mathbf{0}. \quad (42)$$

This approximation is valid when SI channel is strong, the path loss is significant, and the array dimensions M_U and M_D are sufficiently large. It suggests that the design of DL and UL RF beamforming stages, represented by $\mathbf{F}_D$ and $\mathbf{F}_U$ respectively, can effectively eliminate the interference caused by the SI channel. Hence, we conclude that for a given UL-DL angle-pair $\theta_{D_i}, \theta_{U_j}$ in large array structures, the approximation $\mathbf{F}_U\mathbf{H}_{SI}\mathbf{F}_D \approx \mathbf{0}$ holds, indicating the suppression of SI interference.

REFERENCES

[1] M. Mahmood, A. Koc, D. T. Nguyen, R. Morawski, and T. Le-Ngoc, "Sub-array selection in full-duplex massive MIMO for enhanced self-interference suppression," in *Proc. IEEE Glob. Commun. Conf. (GLOBECOM)*, 2023, pp. 5835–5840.

[2] K. E. Kolodziej, B. T. Perry, and J. S. Herd, "In-band full-duplex technology: Techniques and systems survey," *IEEE Trans. Microw. Theory Techn.*, vol. 67, no. 7, pp. 3025–3041, Jul. 2019.

[3] Z. Zhang, K. Long, A. V. Vasilakos, and L. Hanzo, "Full-duplex wireless communications: Challenges, solutions, and future research directions," *Proc. IEEE*, vol. 104, no. 7, pp. 1369–1409, Jul. 2016.

[4] A. Shojaeifard, K.-K. Wong, M. Di Renzo, G. Zheng, K. A. Hamdi, and J. Tang, "Massive MIMO-enabled full-duplex cellular networks," *IEEE Trans. Commun.*, vol. 65, no. 11, pp. 4734–4750, Nov. 2017.

[5] E. Everett, A. Sahai, and A. Sabharwal, "Passive self-interference suppression for full-duplex infrastructure nodes," *IEEE Trans. Wireless Commun.*, vol. 13, no. 2, pp. 680–694, Feb. 2014.

[6] M. S. Sim, M. Chung, D. Kim, J. Chung, D. K. Kim, and C.-B. Chae, "Nonlinear self-interference cancellation for full-duplex radios: From link-level and system-level performance perspectives," *IEEE Commun. Mag.*, vol. 55, no. 9, pp. 158–167, Sep. 2017.

[7] Z. Zhang, X. Chai, K. Long, A. V. Vasilakos, and L. Hanzo, "Full duplex techniques for 5G networks: Self-interference cancellation, protocol design, and relay selection," *IEEE Commun. Mag.*, vol. 53, no. 5, pp. 128–137, May 2015.

[8] B. Debaillie et al., "Analog/RF solutions enabling compact full-duplex radios," *IEEE J. Sel. Areas Commun.*, vol. 32, no. 9, pp. 1662–1673, Sep. 2014.

[9] H. Nawaz and I. Tekin, "Dual-polarized, differential fed microstrip patch antennas with very high interport isolation for full-duplex communication," *IEEE Trans. Antennas Propag.*, vol. 65, no. 12, pp. 7355–7360, Dec. 2017.

[10] C. X. Mao, Y. Zhou, Y. Wu, H. Soewardiman, D. H. Werner, and J. S. Jur, "Low-profile strip-loaded textile antenna with enhanced bandwidth and isolation for full-duplex wearable applications," *IEEE Trans. Antennas Propag.*, vol. 68, no. 9, pp. 6527–6537, Sep. 2020.

[11] D. Korpi, M. Heino, C. Icheln, K. Haneda, and M. Valkama, "Compact inband full-duplex relays with beyond 100 dB self-interference suppression: Enabling techniques and field measurements," *IEEE Trans. Antennas Propag.*, vol. 65, no. 2, pp. 960–965, Feb. 2017.

[12] Y. Liu, P. Roblin, X. Quan, W. Pan, S. Shao, and Y. Tang, "A full-duplex transceiver with two-stage analog cancellations for multipath self-interference," *IEEE Trans. Microw. Theory Techn.*, vol. 65, no. 12, pp. 5263–5273, Dec. 2017.

[13] K. E. Kolodziej, J. G. McMichael, and B. T. Perry, "Multitap RF canceller for in-band full-duplex wireless communications," *IEEE Trans. Wireless Commun.*, vol. 15, no. 6, pp. 4321–4334, Jun. 2016.

[14] J. W. Kwak, M. S. Sim, I.-W. Kang, J. Park, K.-K. Wong, and C.-B. Chae, "Analog self-interference cancellation with practical RF components for full-duplex radios," *IEEE Trans. Wireless Commun.*, vol. 22, no. 7, pp. 4552–4564, Jul. 2023.

[15] E. Ahmed and A. M. Eltawil, "All-digital self-interference cancellation technique for full-duplex systems," *IEEE Trans. Wireless Commun.*, vol. 14, no. 7, pp. 3519–3532, Jul. 2015.
[16] M. A. Islam, G. C. Alexandropoulos, and B. Smida, "Joint analog and digital transceiver design for wideband full duplex MIMO systems," *IEEE Trans. Wireless Commun.*, vol. 21, no. 11, pp. 9729–9743, Nov. 2022.
[17] M. Duarte, C. Dick, and A. Sabharwal, "Experiment-driven characterization of full-duplex wireless systems," *IEEE Trans. Wireless Commun.*, vol. 11, no. 12, pp. 4296–4307, Dec. 2012.
[18] T. Dinc, A. Chakrabarti, and H. Krishnaswamy, "A 60 GHz CMOS full-duplex transceiver and link with polarization-based antenna and RF cancellation," *IEEE J. Solid-State Circuits*, vol. 51, no. 5, pp. 1125–1140, May 2016.
[19] "5G; study on scenarios and requirements for next generation access technologies; Version 17.0.0," 3GPP, Sophia Antipolis, France, Rep. TR 38.913, May 2022.
[20] E. Everett, C. Shepard, L. Zhong, and A. Sabharwal, "SoftNull: Many-antenna full-duplex wireless via digital beamforming," *IEEE Trans. Wireless Commun.*, vol. 15, no. 12, pp. 8077–8092, Dec. 2016.
[21] X. Wu, D. Liu, and F. Yin, "Hybrid beamforming for multi-user massive MIMO systems," *IEEE Trans. Commun.*, vol. 66, no. 9, pp. 3879–3891, Sep. 2018.
[22] P. Zhao and Z. Wang, "Joint user scheduling and hybrid precoding for multi-user mmWave systems with two-layer PS network," in *Proc. IEEE Glob. Commun. Conf. (GLOBECOM)*, 2018, pp. 1–6.
[23] X. Yu, J.-C. Shen, J. Zhang, and K. B. Letaief, "Alternating minimization algorithms for hybrid precoding in millimeter wave MIMO systems," *IEEE J. Sel. Topics Signal Process.*, vol. 10, no. 3, pp. 485–500, Apr. 2016.
[24] A. Koc, A. Masmoudi, and T. Le-Ngoc, "3D angular-based hybrid precoding and user grouping for uniform rectangular arrays in massive MU-MIMO systems," *IEEE Access*, vol. 8, pp. 84689–84712, 2020.
[25] D. Zhang, Y. Wang, X. Li, and W. Xiang, "Hybridly connected structure for hybrid beamforming in mmWave massive MIMO systems," *IEEE Trans. Commun.*, vol. 66, no. 2, pp. 662–674, Feb. 2018.
[26] M. Mahmood, A. Koc, and T. Le-Ngoc, "Energy-efficient MU-massive-MIMO hybrid precoder design: Low-resolution phase shifters and digital-to-analog converters for 2D antenna array structures," *IEEE Open J. Commun. Soc.*, vol. 2, pp. 1842–1861, 2021.
[27] M. Mahmood, A. Koc, and T. Le-Ngoc, "2D antenna array structures for hybrid massive MIMO precoding," in *Proc. IEEE Glob. Commun. Conf. (GLOBECOM)*, 2020, pp. 1–6.
[28] M. Mahmood, A. Koc, and T. Le-Ngoc, "Massive-MIMO hybrid precoder design using few-bit DACs for 2D antenna array structures," in *Proc. IEEE Int. Conf. Commun. (ICC)*, 2021, pp. 1–5.
[29] M. Mahmood, A. Koc, and T. Le-Ngoc, "3-D antenna array structures for millimeter wave multi-user massive MIMO hybrid precoder design: A performance comparison," *IEEE Commun. Lett.*, vol. 26, no. 6, pp. 1393–1397, Jun. 2022.
[30] Y. Gong, M. Mahmood, R. Morawski, and T. Le-Ngoc, "Dual-layer metamaterial rectangular antenna arrays for in-band full-duplex massive MIMO," *IEEE Access*, vol. 11, pp. 135708–135727, 2023.
[31] A. Koc and T. Le-Ngoc, "Full-duplex mmWave massive MIMO systems: A joint hybrid Precoding/combining and self-interference cancellation design," *IEEE Open J. Commun. Soc.*, vol. 2, pp. 754–774, 2021.
[32] S. Huberman and T. Le-Ngoc, "MIMO full-duplex precoding: A joint beamforming and self-interference cancellation structure," *IEEE Trans. Wireless Commun.*, vol. 14, no. 4, pp. 2205–2217, Apr. 2015.
[33] Y. Zhang, M. Xiao, S. Han, M. Skoglund, and W. Meng, "On precoding and energy efficiency of full-duplex millimeter-wave relays," *IEEE Trans. Wireless Commun.*, vol. 18, no. 3, pp. 1943–1956, Mar. 2019.
[34] Z. Luo, L. Zhao, L. Tonghui, H. Liu, and R. Zhang, "Robust hybrid precoding/combining designs for full-duplex millimeter wave relay systems," *IEEE Trans. Veh. Technol.*, vol. 70, no. 9, pp. 9577–9582, Sep. 2021.
[35] A. Koc and T. Le-Ngoc, "Intelligent non-orthogonal beamforming with large self-interference cancellation capability for full-duplex multiuser massive MIMO systems," *IEEE Access*, vol. 10, pp. 51771–51791, 2022.
[36] K. Satyanarayana, M. El-Hajjar, P.-H. Kuo, A. Mourad, and L. Hanzo, "Hybrid beamforming design for full-duplex millimeter wave communication," *IEEE Trans. Veh. Technol.*, vol. 68, no. 2, pp. 1394–1404, Feb. 2019.
[37] I. P. Roberts, J. G. Andrews, and S. Vishwanath, "Hybrid beamforming for millimeter wave full-duplex under limited receive dynamic range," *IEEE Trans. Wireless Commun.*, vol. 20, no. 12, pp. 7758–7772, Dec. 2021.
[38] Y. Cai, K. Xu, A. Liu, M. Zhao, B. Champagne, and L. Hanzo, "Two-timescale hybrid analog-digital beamforming for mmWave full-duplex MIMO multiple-relay aided systems," *IEEE J. Sel. Areas Commun.*, vol. 38, no. 9, pp. 2086–2103, Sep. 2020.
[39] Y. Chen, D. Chen, T. Jiang, and L. Hanzo, "Millimeter-wave massive MIMO systems relying on generalized sub-array-connected hybrid precoding," *IEEE Trans. Veh. Technol.*, vol. 68, no. 9, pp. 8940–8950, Sep. 2019.
[40] M. Mahmood, Y. Zhang, R. Morawski, and T. Le-Ngoc, "Adaptive modulus RF beamforming for enhanced self-interference suppression in full-duplex massive MIMO systems," in *Proc. IEEE Wireless Commun. Netw. Conf. (WCNC)*, 2024, pp. 1–6.
[41] C. Lin, G. Y. Li, and L. Wang, "Subarray-based coordinated beamforming training for mmWave and sub-THz communications," *IEEE J. Sel. Areas Commun.*, vol. 35, no. 9, pp. 2115–2126, Sep. 2017.
[42] C. Lin and G. Y. Li, "Energy-efficient design of indoor mmWave and sub-THz systems with antenna arrays," *IEEE Trans. Wireless Commun.*, vol. 15, no. 7, pp. 4660–4672, Jul. 2016.
[43] X. Song, T. Kühne, and G. Caire, "Fully-/partially-connected hybrid beamforming architectures for mmWave MU-MIMO," *IEEE Trans. Wireless Commun.*, vol. 19, no. 3, pp. 1754–1769, Mar. 2020.
[44] X. Cheng et al., "Communicating in the real world: 3D MIMO," *IEEE Wireless Commun.*, vol. 21, no. 4, pp. 136–144, Aug. 2014.
[45] Y. Gong, R. Morawski, H. H. Lee, and T. Le-Ngoc, "A miniaturized 8x8 dual-layer EBG slotted circularly polarized patch antenna array for mMIMO," in *Proc. IEEE Glob. Commun. Conf. (GLOBECOM)*, 2022, pp. 6511–6516.
[46] "5G; NR;. base station (BS) radio transmission and reception; Version 16.4.0," 3GPP, Sophia Antipolis, France, Rep. TS 38.104, Jul. 2020.
[47] "5G; study on channel model for frequencies from 0.5 to 100 GHz; Version 16.1.0," 3GPP, Sophia Antipolis, France, Rep. TR 38.901, Nov. 2020.

MOBEEN MAHMOOD (Graduate Student Member, IEEE) received the B.Sc. degree (Hons.) in electrical engineering from the University of Engineering and Technology, Taxila, Pakistan, in 2013, and the M.Sc. degree (Hons.) in electrical engineering from the American University of Sharjah (AUS), Sharjah, UAE, in 2019. He is currently pursuing the Ph.D. degree in electrical engineering with McGill University, Montreal, QC, Canada.

From 2014 to 2017, he was with China Mobile Pakistan, Islamabad, Pakistan. His main research interests include massive MIMO, hybrid beamforming, AI-enabled wireless networks, UAV, and full-duplex communications. He is the recipient of the AUS Teaching Assistantship, the AUS Research Assistantship, the Fonds de Recherche du Québec-Nature and Technologies, the IEEE VTS Student Travel Award, the IEEE Canada Vehicular Technologies Grant, the McGill Graduate Research Enhancement and Travel Award, the McGill Graduate Excellence Fellowship, the McGill Engineering Class of 1936 Fellowship, and the J.W.McConnell Memorial Fellowship as part of McGill Engineering Doctoral Award.

ASIL KOC (Graduate Student Member, IEEE) received the B.Sc. degree (Hons.) in electronics and communication engineering and the M.Sc. degree (Hons.) in telecommunication engineering from Istanbul Technical University, Istanbul, Turkey, in 2015 and 2017, respectively, and the Ph.D. degree in electrical engineering from McGill University, Montreal, Canada, in 2022.

From 2015 to 2017, he was a Research and Teaching Assistant with the Electronics and Communication Engineering Department, Istanbul Technical University. From 2017 to 2022, he was a Lecturer and a Teaching Assistant with the Electrical and Computer Engineering Department, McGill University. In 2022, he worked as a Mitacs Accelerate Intern with Huawei Technologies Canada. His research interests include AI/ML-based wireless communications, massive MIMO, full-duplex, millimeter-wave/terahertz, beamforming, and reconfigurable intelligent surface. He was a recipient of the Erasmus Scholarship by European Union, the McGill Engineering Doctoral Award, the IEEE ComSoc Student Travel Grant, the Graduate Research Enhancement and Travel Award by McGill University, and the STARaCom Collaborative Grant by the FRQNT.

ROBERT MORAWSKI received the B.Sc. and M.Sc. degrees in electrical and computer engineering from Concordia University, Montreal, Canada, in 1997 and 2000, respectively. He is currently a Research Engineer and a Lab Manager with the Broadband Communications Research Lab, ECE Department, McGill University, Montreal. His research interests include the design and implementation of prototype architectures for next-generation wireless communications.

THO LE-NGOC (Life Fellow, IEEE) received the B.Eng. degree in electrical engineering and the M.Eng. degree in microprocessor applications from McGill University, Montreal, in 1976 and 1978, respectively, and the Ph.D. degree in digital communications from the University of Ottawa, Canada, in 1983. From 1977 to 1982, he was with Spar Aerospace Ltd., Sainte-Anne-de-Bellevue, QC, Canada, involved in the development and design of satellite communications systems. From 1982 to 1985, he was with SRTelecom Inc., Saint-Laurent, QC, Canada, where he developed the new point-to-multipoint DA-TDMA/TDM Subscriber Radio System SR500. From 1985 to 2000, he was a Professor with the Department of Electrical and Computer Engineering, Concordia University, Montreal. Since 2000, he has been with the Department of Electrical and Computer Engineering, McGill University. His research interest includes broadband digital communications. He was a recipient of the 2004 Canadian Award in Telecommunications Research and the IEEE Canada Fessenden Award in 2005. He is a Distinguished James McGill Professor, and a Fellow of the Engineering Institute of Canada, the Canadian Academy of Engineering, and the Royal Society of Canada.